Supplemental Materials

Multi-Omics Analysis of the NAD^+-PARP1 Axis Reveals a Role for Site-Specific ADP-ribosylation in Splicing in Embryonic Stem Cells

Aarin Jones and W. Lee Kraus

Contains:
- Supplemental Figures S1 through S15 and legends
- Legends for Supplemental Tables S1 through S4
- Supplemental Materials and Methods
- Supplemental References

Also, included separately as Excel spreadsheets:
- Supplemental Tables S1 through S4

SUPPLEMENTAL FIGURES AND LEGENDS

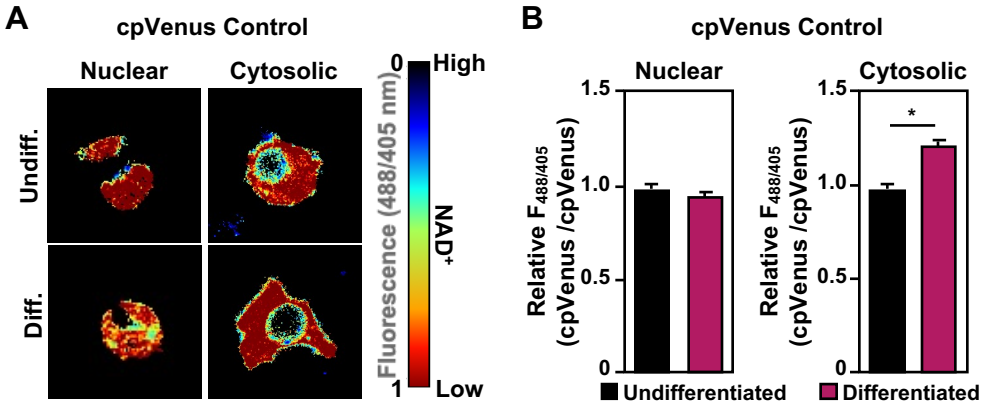

Supplemental Figure S1. Differentiation does not affect the fluorescence intensities of the cpVenus control sensors.
(A) Fluorescence images of cpVenus control sensors in undifferentiated (Undiff.) and 12 hour differentiated (Diff.) WT mESCs. The mESCs were transfected with the cpVenus control plasmids and then imaged by fluorescent microscopy. The scale bar indicates fluorescence (488/405nm) ratios and the corresponding NAD^+ levels.
(B) Quantification of multiple experiments like those shown in (A). Each bar in the graph represents the mean ± SEM of differentiated $control_{(488/405\ nm)}$/undifferentiated $control_{(488/405\ nm)}$ fluorescence ratios determined by live cell imaging (n = 3; ANOVA, $*p < 0.05$, $**p < 0.01$, $***p < 0.001$, $****p < 0.0001$).

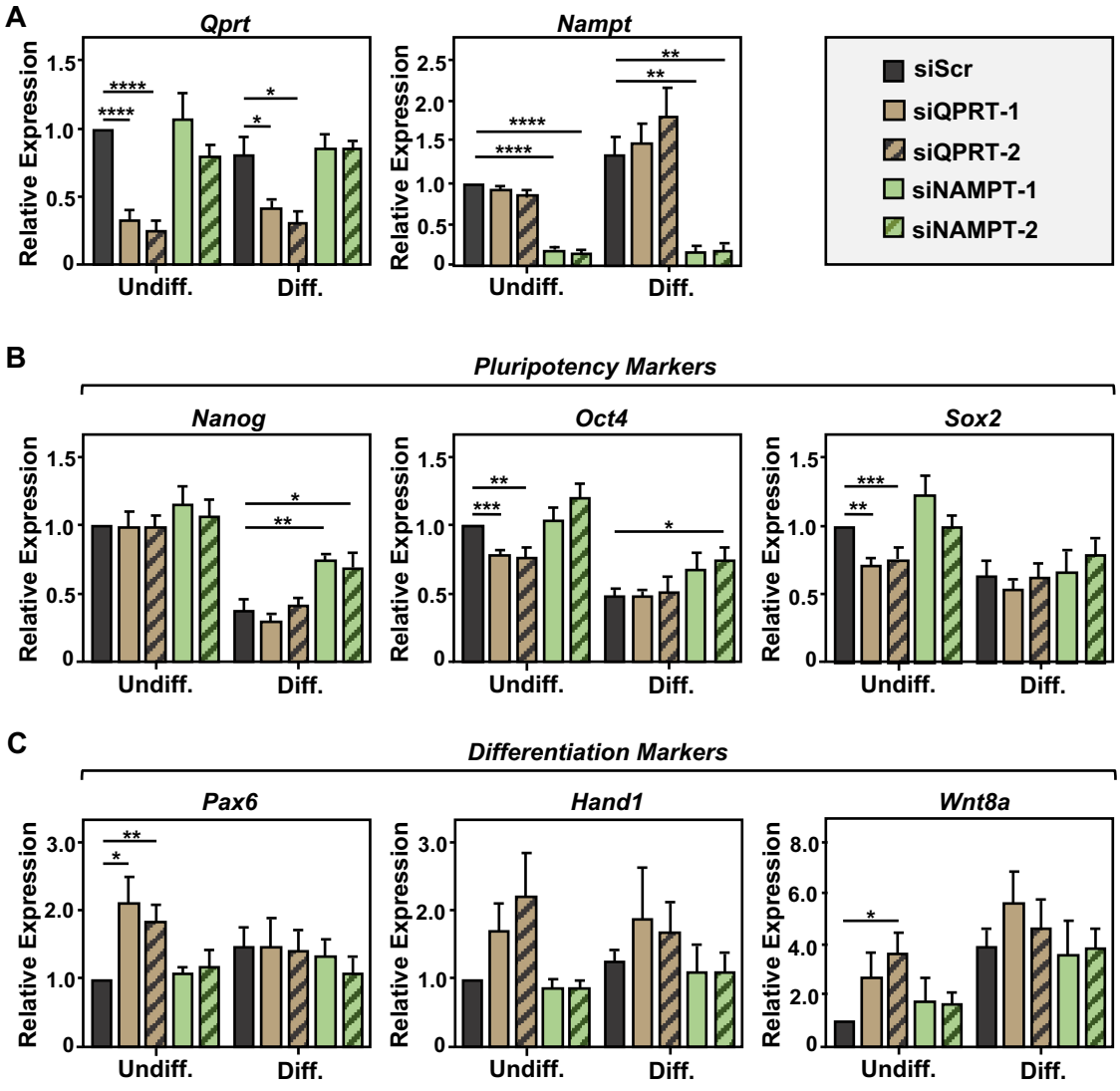

Supplemental Figure S2. Depletion of key enzymes in NAD$^+$ biosynthetic pathways disrupts the maintenance of pluripotency when the pathway are most active.

Expression levels of canonical pluripotency and differentiation marker genes in mESCs upon siRNA-mediated depletion of QPRT or NAMPT (key De novo and Salvage pathway enzymes, respectively) before and after 12 hours of differentiation. The expression of the genes was quantified by RT-qPCR ($n \geq 4$, multiple unpaired t-test, $^{*}p < 0.05$, $^{**}p < 0.01$, $^{***}p < 0.001$, $^{****}p < 0.0001$).

(A) Assays confirming knockdown of *Qprt1* and *Nampt*. The key for the experimental conditions is show at the right.

(B) Expression of pluripotency marker genes.

(C) Expression of differentiation marker genes.

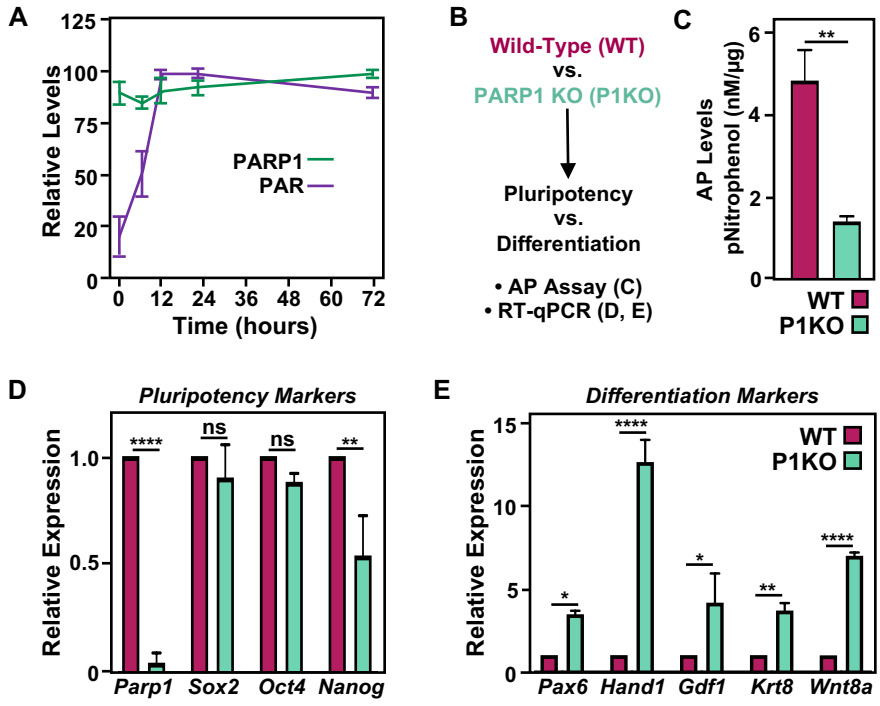

Supplemental Figure S3. P1KO mESCs exist in a unique metastable pluripotent state.
(A) Quantification of Western blots of PAR and PARP1 in WT mESCs over a time course of differentiation like those shown in Figure 3A, *left*. Each point in the graph represents the mean ± SEM ($n \geq 3$).
(B) Schematic of the experimental plan and assays for assessing the effects of genetic deletion of *Parp1* in mESCs.
(C) Assay showing the activity of pluripotency marker enzyme alkaline phosphatase in WT and P1KO mESCs. ($n = 4$; ANOVA, $**p < 0.01$).
(D and E) Expression levels of canonical pluripotency (D) and differentiation (E) marker genes upon genetic deletion of *Parp1* in mESCs, as assessed by RT-qPCR ($n = 3$; ANOVA, $*p < 0.05$, $**p < 0.01$, $****p < 0.0001$; ns = not significant).

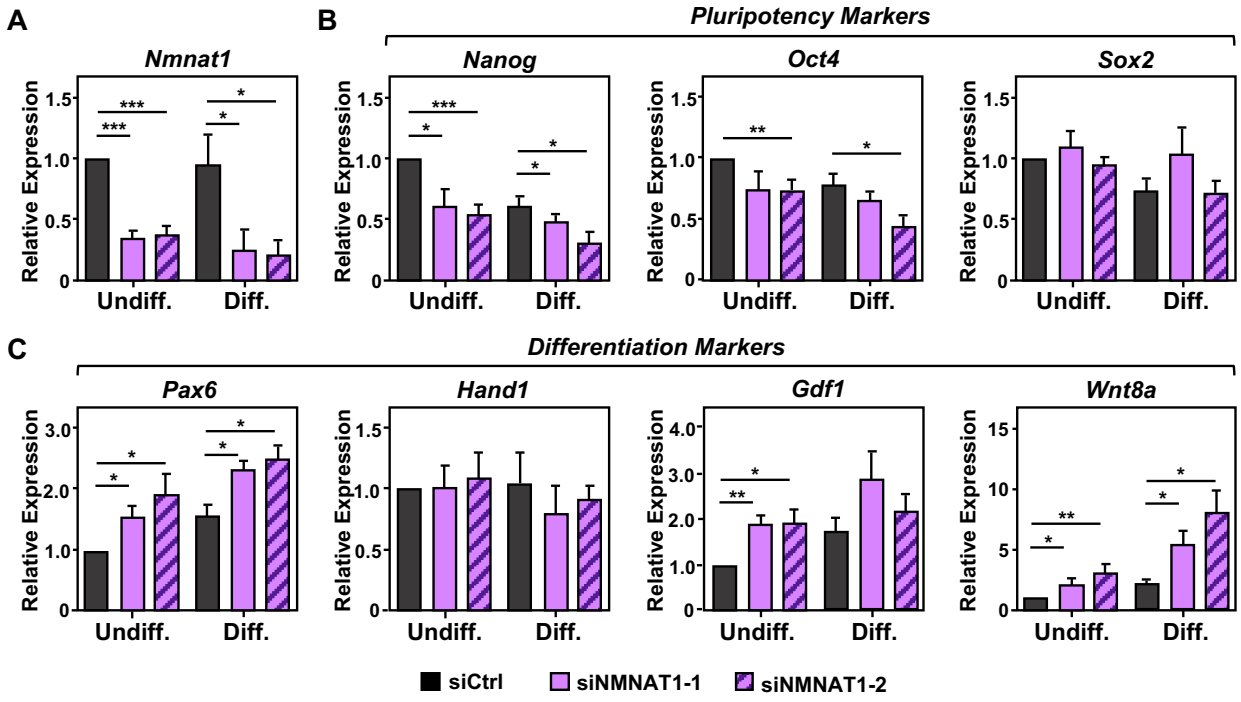

Supplemental Figure S4. Depletion of NMNAT1 alters mESC pluripotency.
Expression levels of canonical pluripotency and differentiation marker genes in mESCs upon siRNA-mediated depletion of NMNAT1 before and after 24 hours of differentiation. The expression of the genes was quantified by RT-qPCR ($n \geq 3$, multiple unpaired t-test, $^{*}p < 0.05$, $^{**}p < 0.01$, $^{***}p < 0.001$, $^{****}p < 0.0001$).
(A) Assay confirming knockdown of *Nmnat1*.
(B) Expression of pluripotency marker genes.
(C) Expression of differentiation marker genes.

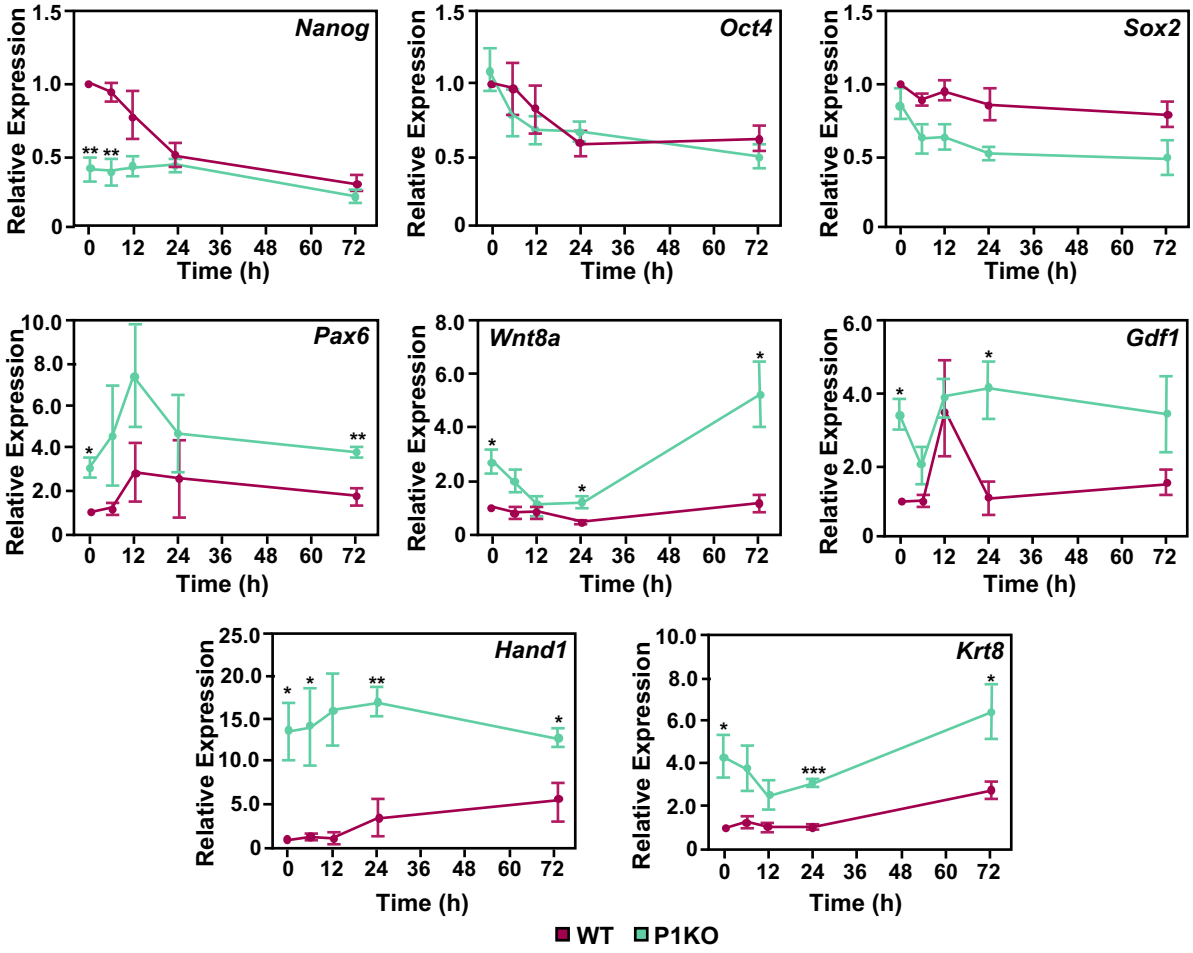

Supplemental Figure S5. P1KO mESCs are capable of differentiation as assessed by marker gene expression.

Expression levels of canonical pluripotency and differentiation markers in WT and P1KO mESCs during a time course of differentiation. The expression of the genes was quantified by RT-qPCR. ($n \geq 3$, two-way ANOVA, Sidak, $^{*}p < 0.05$, $^{**}p < 0.01$, $^{***}p < 0.001$, $^{****}p < 0.0001$).

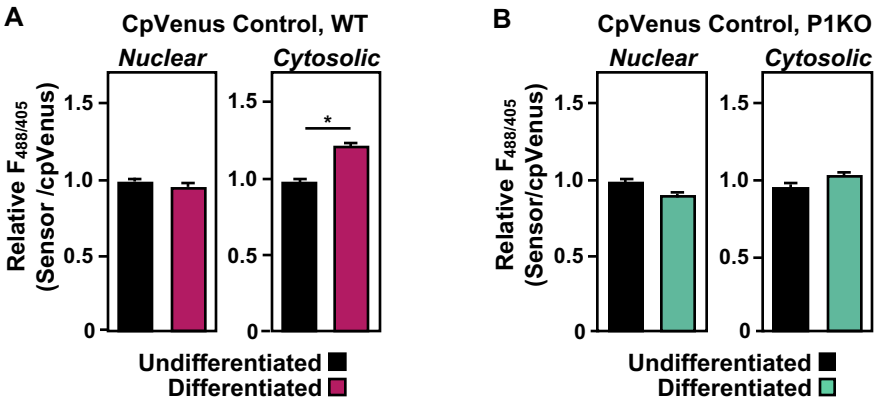

Supplemental Figure S6. Differentiation or genetic deletion of *Parp1* has little to no effect on the fluorescence intensities of the cpVenus control sensors.

These experiments are controls for the experiments shown in Figure 3, C and D. Each bar in the graphs represents the mean ± SEM of differentiated control$_{(488/405\ nm)}$/undifferentiated control$_{(488/405\ nm)}$ fluorescence ratios determined by live cell imaging using (n = 3; ANOVA, *p < 0.05). Note that the data for WT mESCs is repeated from Figure S1B for comparison.

(A) Effect of differentiation on the fluorescence intensities of the cpVenus control sensors in WT mESCs.

(B) Effect of genetic deletion of *Parp1* on the fluorescence intensities of the cpVenus control sensors using P1KO mESCs.

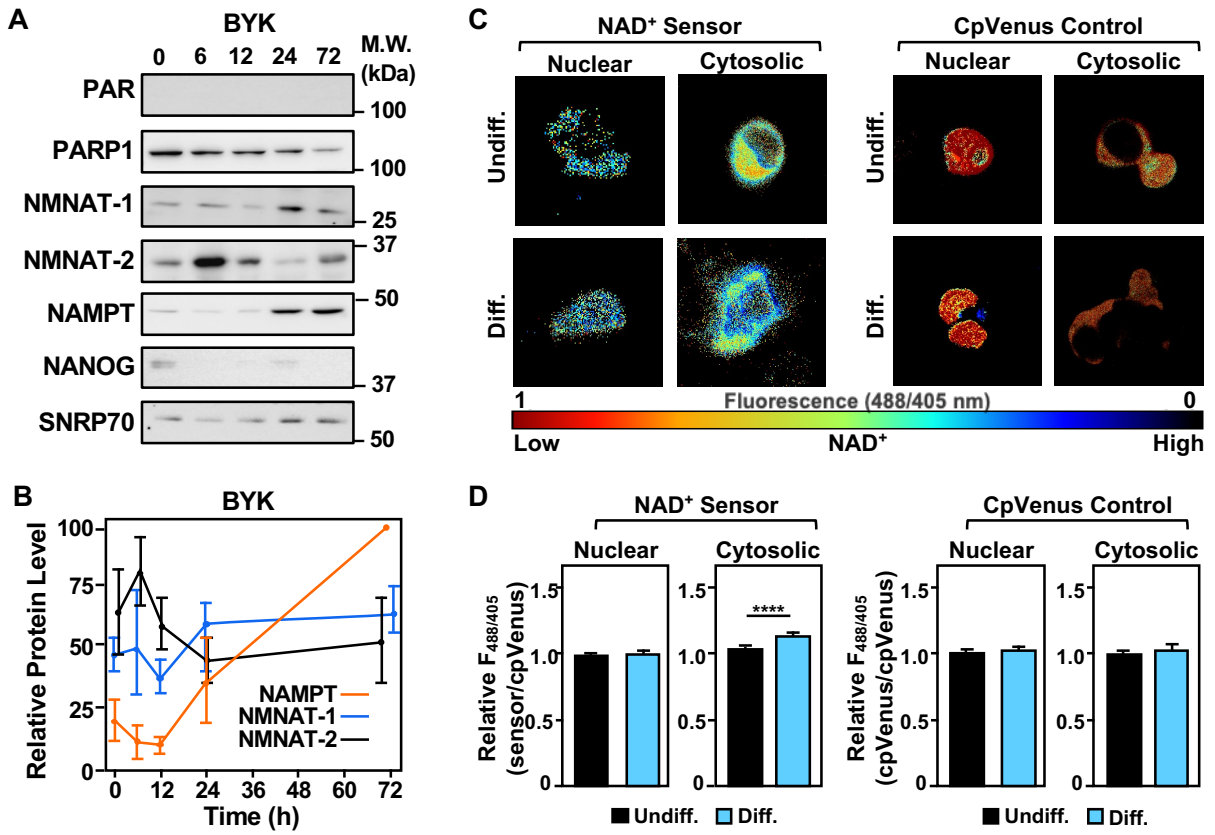

Supplemental Figure S7. Treatment of mESCs with PARP inhibitor alters the levels of NAD$^+$ biosynthetic enzymes and NAD$^+$ compartmentalization in a manner similar to that of *Parp1* knockout.

(A) Western blot analysis of whole cell extracts prepared from BYK204165 (BYK)-treated mESCs during a time course of differentiation as indicated (compare to Figure 3A). The levels of NANOG and SNRP70 were used as markers for differentiation and loading, respectively.

(B) Quantification of Western blots for NAMPT, NMNAT-1, and NMNAT-2 assessing their levels during a time course of differentiation in BYK-treated mESCs (compare to Figures 1B and 3B).

(C and D) Compartment-specific NAD$^+$ levels in undifferentiated mESCs (Undiff.) or mESCs differentiated by LIF removal for 12 hours (Diff.) treated with the PARP inhibitor Veliparib. The fluorescence images in (C) were generated using nuclear and cytosolic NAD$^+$ sensors as indicated. The scale bar shows the inverse relationship between fluorescent signal and NAD$^+$ levels. *Left*, Sensor; *Right*, cpVenus control. The bars in the graphs in (D) represent the mean ± SEM of the relative NAD$^+$ concentrations calculated using sensor$_{(488/405\ nm)}$/control$_{(488/405\ nm)}$ fluorescence ratios determined by live cell imaging (n = 3, ANOVA, $^{**}p < 0.01$, $^{***}p < 0.001$, $^{****}p < 0.0001$).

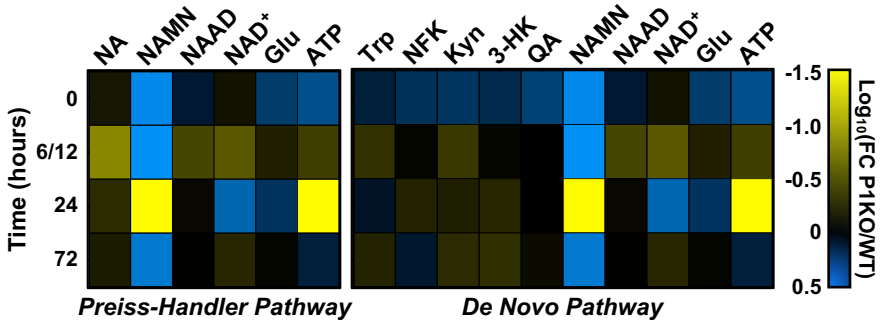

Supplemental Figure S8. Analysis of NAD$^+$ pathway metabolites in P1KO mESCs during a time course of differentiation.

Heat map representation of the levels of metabolites involved in the NAD$^+$ biosynthetic pathways in P1KO mESCs during a time course of differentiation by LIF removal as determined by mass spectrometry. Each row represents a single metabolite throughout the time course. Metabolites that increased in P1KO mESCs versus WT mESCs at the same time point of differentiation are represented in blue (Log_{10} fold change; FC). Metabolites that decreased in abundance are indicated in yellow. Metabolites are grouped and ordered according to the NAD$^+$ metabolic pathways (Preiss-Handler and de novo), as indicated.

Supplemental Figure S9. Identification of PARP1 substrates in mESCs using an NAD^+ analog-sensitive PARP1 (asPARP1) approach.
(A) Schematic representation of the asPARP approach using a single bi-functional and "clickable" NAD^+ analog.
(B) Chemical structure of the clickable NAD^+ analog 8-Bu(3-yne)T-NAD^+.
(C) SDS-PAGE analysis with subsequent Coomassie blue staining of purified FLAG-tagged wild-type PARP1 (WT) and analog-sensitive PARP1 (L877A; AS) expressed in Sf9 insect cells and purified using FLAG affinity chromatography. Three eluates for each and molecular weight markers in kDa are shown.
(D) In vitro PARylation assays with wild-type PARP1 (WT) and analog-sensitive PARP1 (L877A; AS) in the presence of NAD^+ or 8-Bu(3-yne)T-NAD^+. Western blots with a PAR detection reagent were used to assess the levels of auto-modified PARP1. Molecular weight markers in kDa are shown.
(E) In-gel fluorescence assay of nuclear extract proteins from WT mESCs subjected to in vitro PARylation by wild-type PARP1 (WT) and analog-sensitive PARP1 (L877A; AS) in the presence NAD^+ or 8-Bu(3-yne)T-NAD^+. The products were conjugated to azido-TAMRA and analyzed by SDS-PAGE with subsequent fluorescence detection. Molecular weight markers in kDa are shown.
(F) Venn diagram showing the overlap of protein substrates among multiple replicates of asPARP1 LC-MS/MS substrate determination.

[See Supplemental Figure S9 on the next page]

Supplemental Figure S9.

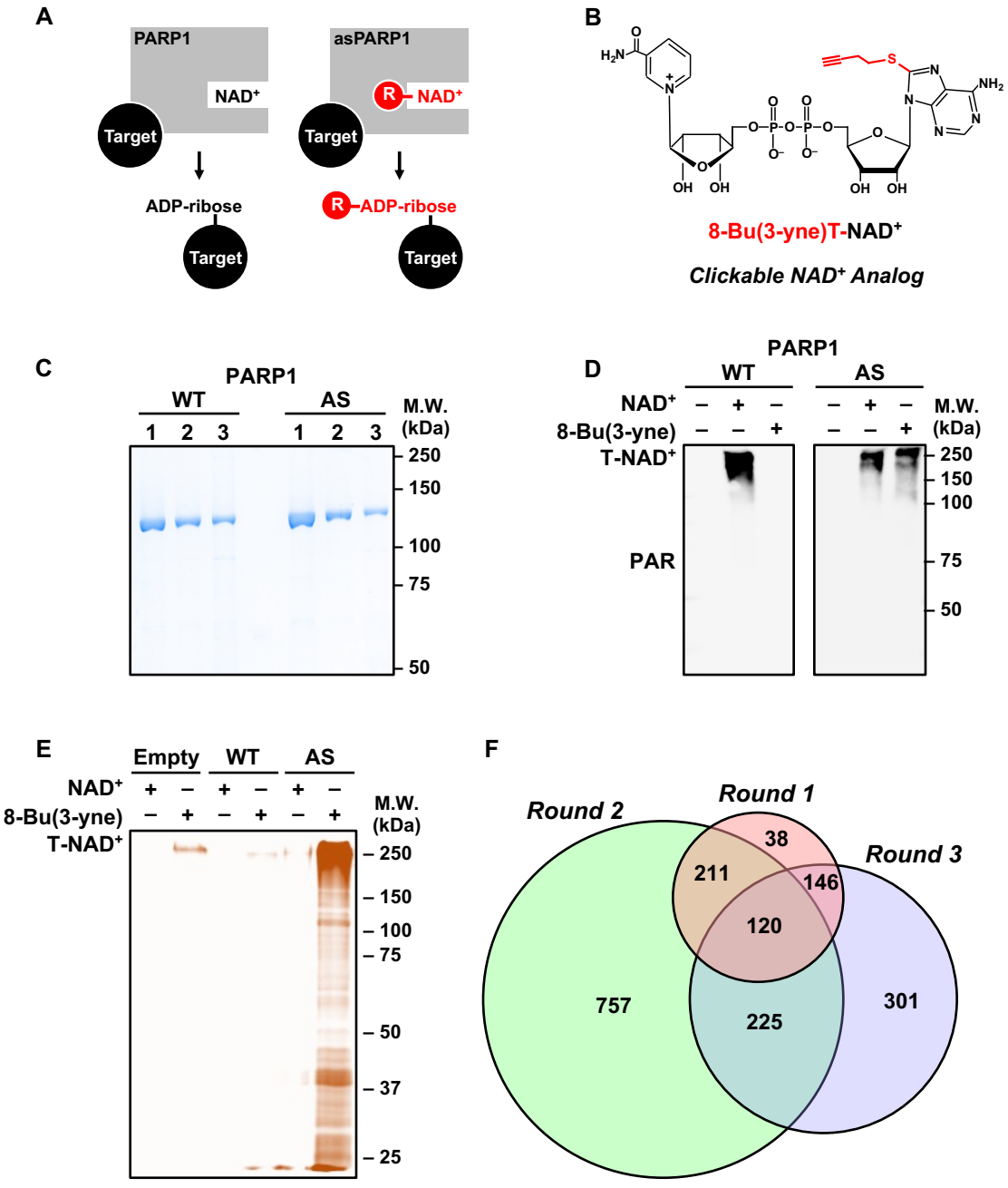

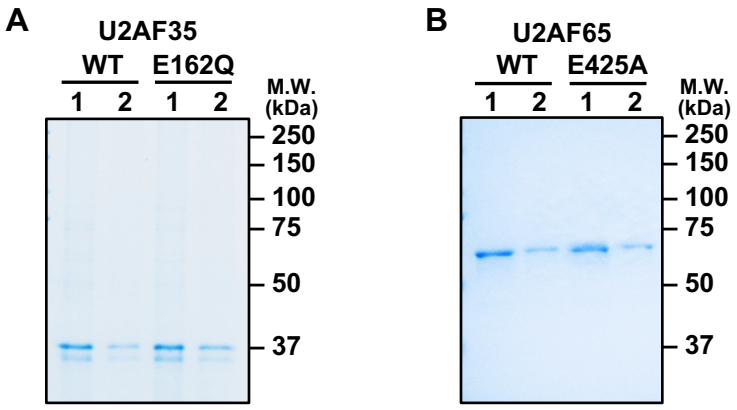

Supplemental Figure S10. Expression and purification of wild-type and ADPRylation site mutant U2AF35 and U2AF65.
(A and B) SDS-PAGE analysis with subsequent Coomassie blue staining of purified FLAG-tagged wild-type (WT) and mutant U2AF proteins expressed in Sf9 insect cells and purified using FLAG affinity chromatography. Two eluates for each and molecular weight markers in kDa are shown. (A) WT and E162Q U2AF35. (B) WT and E425A U2AF65.

Supplemental Figure S11. U2AF35 and U2AF65 are PARylated in mESCs during differentiation, plus control experiments for the RNA EMSAs.
(A and C) Quantification of in vitro PARylation assays from Figure 5, A and B, with WT or ADPRylation site mutant (E162Q) U2AF35 in the presence of PARP1 and NAD^+. (A) Assay with U2AF35 WT versus E162Q. (C) Assay with RNA oligonucleotides containing either a strong U2 splice site acceptor or a U12 class splice site. ($n \geq 4$, two-tailed unpaired t-test, $^{*}p < 0.05$, $^{**}p < 0.01$, $^{***}p < 0.001$, $^{****}p < 0.0001$).
(B) WT mESCs were transfected with expression constructs for wild-type or ADPRylation site mutant Flag-tagged U2AF35 (WT or E162Q) and then differentiated for twelve hours. The Flag-tagged U2AF35 protein was immunoprecipitated (IP) from the cells. The input and the IP'ed material were subjected to Western blotting for PAR, PARP1, FLAG, Actin, or U2AF35 as indicated.
(C and D) Quantification of in vitro PARylation assays from Figure 5, C and D, with WT or ADPRylation site mutant (E425A) U2AF65 in the presence of PARP1 and NAD^+. (C) Assay with U2AF65 WT versus E425A. (D) Assay with RNA oligonucleotides containing either a strong U2 splice site acceptor sequence or a U12 class splice site. ($n \geq 4$, two-tailed unpaired t-test, $^{*}p < 0.05$, $^{**}p < 0.01$, $^{***}p < 0.001$, $^{****}p < 0.0001$).
(E) WT mESCs were transfected with expression constructs for wild-type or ADPRylation site mutant Flag-tagged U2AF65 (WT or E425A) and then differentiated for twelve hours. The Flag-tagged U2AF65 protein was immunoprecipitated (IP) from the cells. The input and the IP'ed material were subjected to Western blotting for PAR, PARP1, FLAG, Actin, or U2AF65 as indicated.
(E and F) RNA EMSAs with purified WT or ADP-ribosylation site mutant (E425A) U2AF65. Cy5-labeled *Lpl* or Cy5-labeled *Scn8a* RNAs containing 3' splice sites in the binding reactions. The binding reactions were run on a native 6% polyacrylamide gel in 1x TBE and then imaged directly using a ChemiDoc MP system. (E) Comparing the sequence specificity and ability of WT or ADP-ribosylation site mutant (E425A) U2AF65 to bind to the *Lpl* and *Scn8a* splice sites in the absence of PARylation. (F) Testing the ability of U2AF65 to bind to the *Lpl* splice site in PARylation Reaction Buffer.

[See Supplemental Figure S11 on the next page]

Supplemental Figure S11.

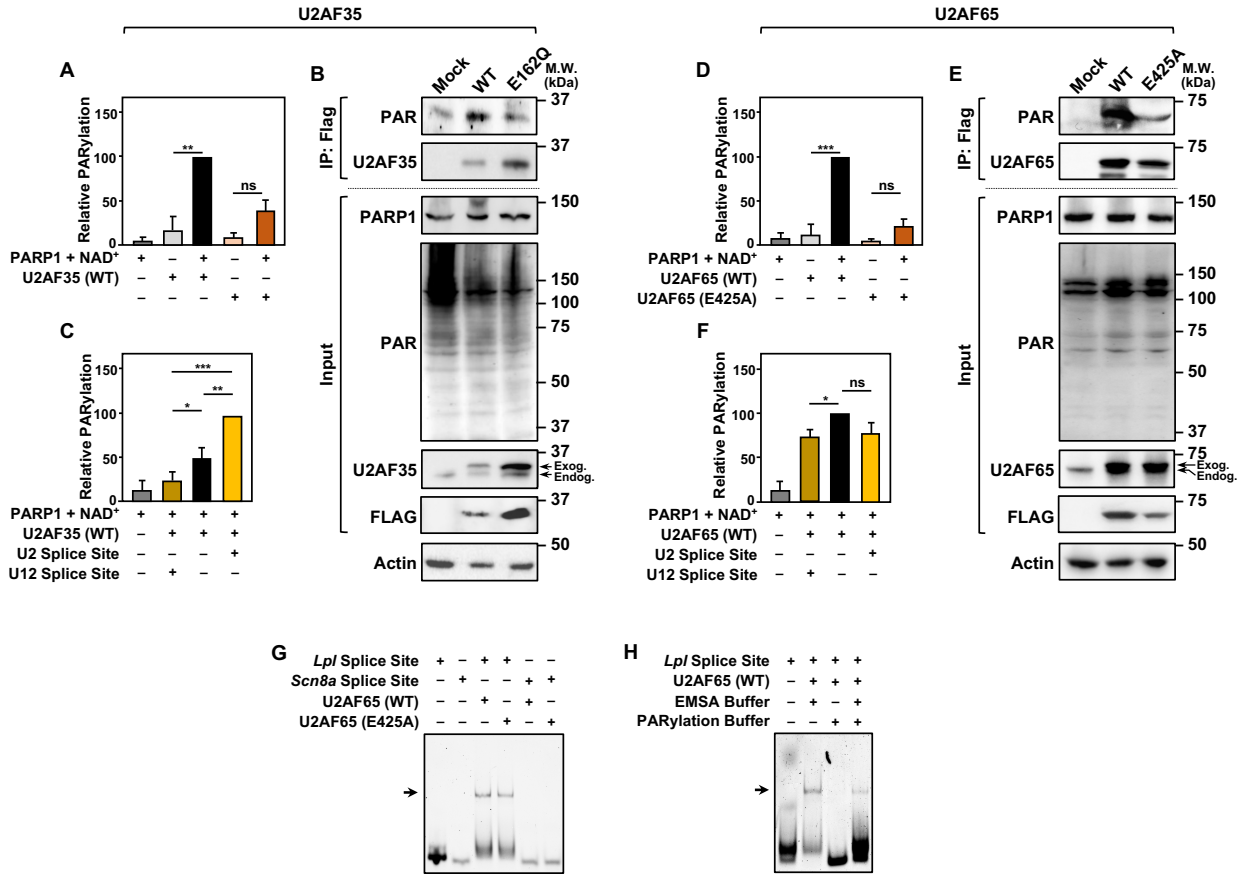

Supplemental Figure S12. Genetic depletion of PARP1 in mESCs alters cell state-dependent splicing patterns.
(A) *Left*, Schematic representation of a segment of the *Ctnnd1* gene illustrating two exon skipping events that distinguish between two isoforms of the *Ctnnd1* mRNA (3a and 4a). Isoform 3a is predominant in the pluripotent state, while isoform 4a is predominant during differentiation. Two sets of PCR primers (F1/R1 and F2/R2) can be used to amplify PCR products that distinguish between the two isoforms. *Right*, Expected sizes of the PCR products for each isoform produced using the two sets of primers.
(B) Semi-quantitative PCR of *Ctnnd1* isoforms 3a and 4a using total RNA isolated from WT and P1KO mESCs and the non-overlapping primer sets shown in (A). The products were run on a 2% agarose gel and stained with Sybr Safe for visualization. Molecular size markers in bp are shown. The products are labeled and color-coded as indicated. At 0 hours of differentiation, P1KO mESCs have lower expression of isoform 3a and higher expression of isoform 4a versus WT mESCs.
(C) Splicing distribution plot of significantly altered splicing events by splicing class at 12 hours of differentiation in WT and P1KO mESCs. The proportion of each type of splicing event is indicated. SE, skipped exon; RI, retained intron; MXE, mutually exclusive exons; A5SS, alternative 5' splice sites; A3SS, alternative 3' splice sites.
(D) Line plot representation showing percent of significantly altered retained intron splicing events in mESCs over a time course of differentiation comparing WT and P1KO mESCs. Events at each time point are expressed relative to undifferentiated (0 hour) WT or P1KO. Percent significantly ASEs were calculated by dividing statistically significant events (ΔPSI > 0.2 and Bayes Factor > 5) by the total number of splicing events at each time point and multiplying by 100.
(E) Violin plots illustrating significantly altered splicing events (ASEs) in WT and P1KO mESCs at 12 hours differentiation upon LIF removal. (*left*) A5SS, alternative 5' splice sites (106 splicing events), (*middle*) A3SS, alternative 3' splice sites (219 splicing events), (*right*) MXE, mutually exclusive exons (48 splicing events). Significantly altered splicing events were defined as a ΔPSI > 0.1 and FDR = 0.05.

[See Supplemental Figure S12 on the next page]

Supplemental Figure S12.

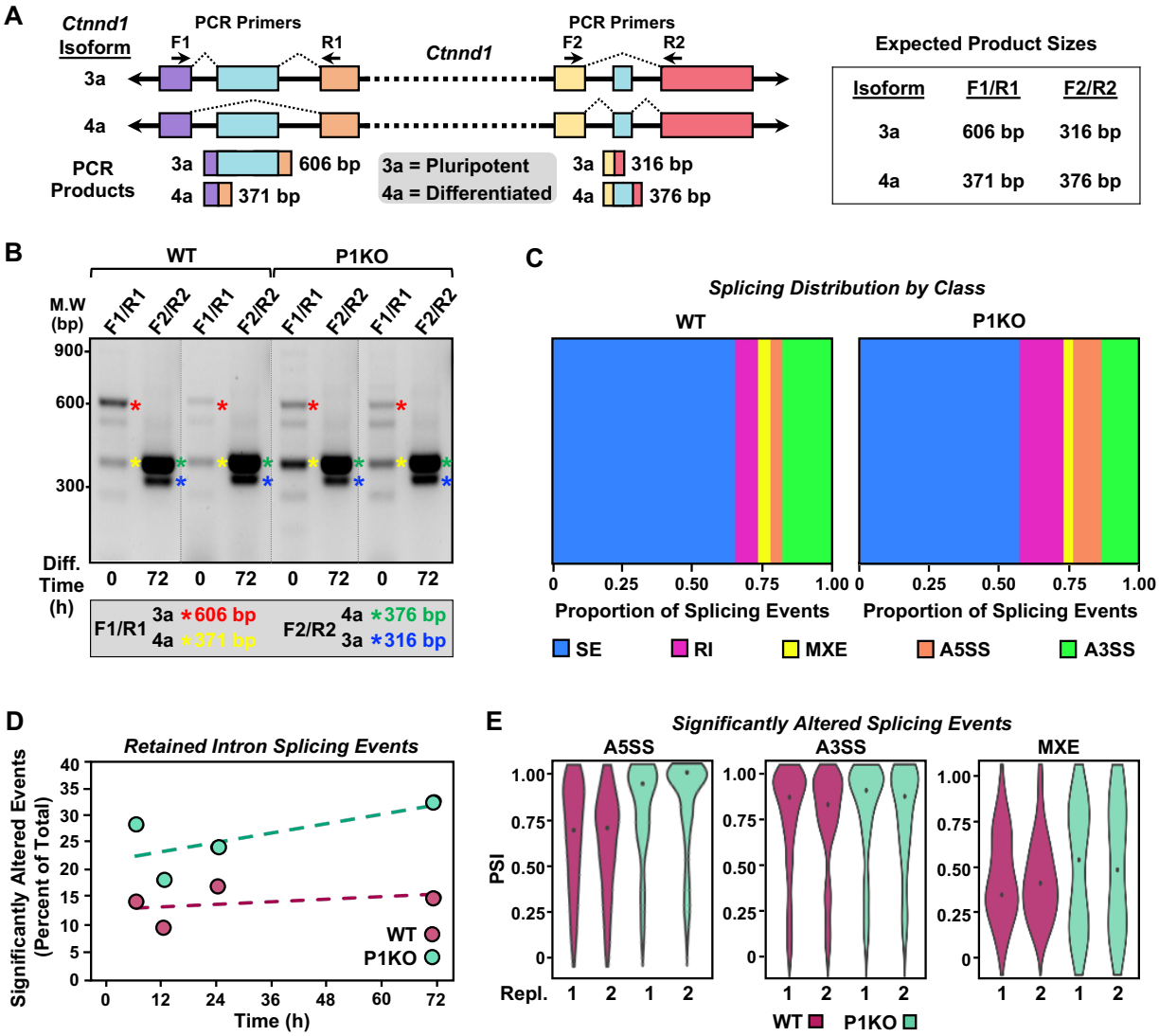

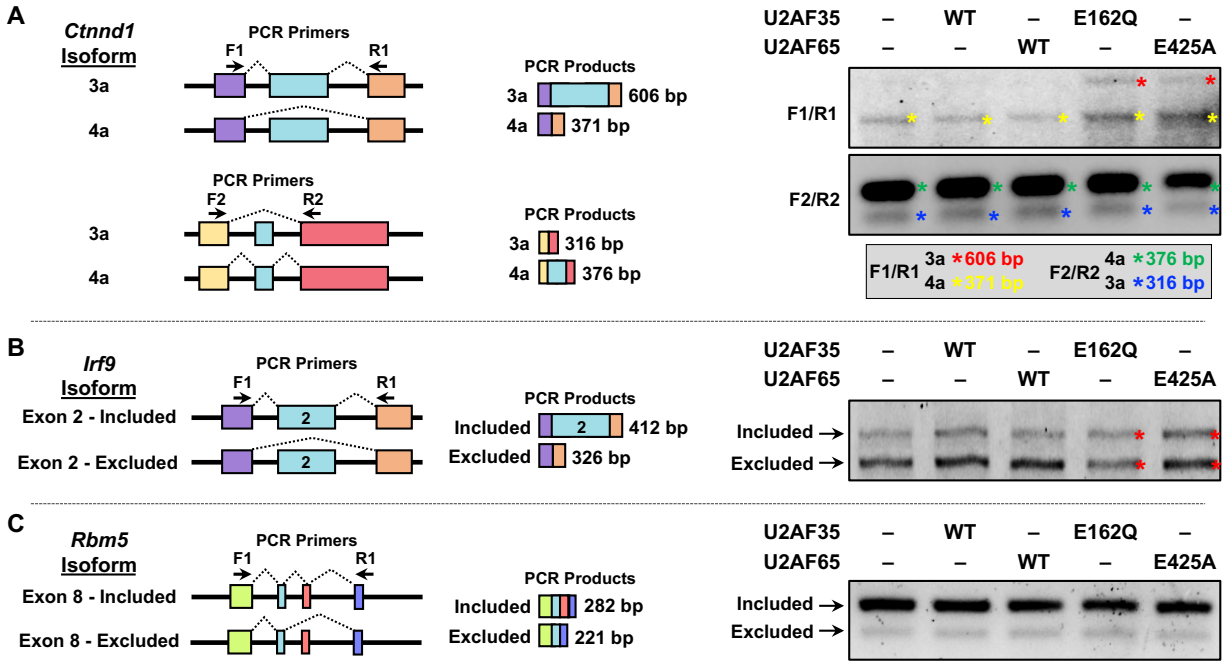

Supplemental Figure S13. Expression of ADPRylation deficient U2AF mutants alter splicing.
(A) *Left*, Schematic representation of a segment of the *Ctnnd1* gene illustrating exon skipping events that distinguish between two isoforms of the *Ctnnd1* mRNA (3a and 4a). Isoform 3a is predominant in the pluripotent state, while isoform 4a is predominant during differentiation. Two sets of PCR primers (F1/R1 and F2/R2) were used to amplify PCR products that distinguish between the two isoforms. *Right*, Semi-quantitative PCR of *Ctnnd1* isoforms 3a and 4a using total RNA isolated from WT mESCs expressing WT or ADPRylation site mutant U2AFs differentiated for 12 hours. Colored asterisks indicate the sizes of the PCR products indicated in the key (*bottom*).
(B) *Left*, Schematic representation of a segment of the *Irf9* gene illustrating skipping of exon 2. *Irf9* splicing was identified as altered by RNA-seq. *Right*, Semi-quantitative PCR of *Irf9* isoforms using total RNA isolated from WT mESCs expressing WT or ADPRylation site mutant U2AFs differentiated for 12 hours. Asterisks indicate an increased included/excluded ratio.
(C) *Left*, Schematic representation of a segment of the *Rbm5* gene illustrating exon skipping of exon 8. *Rbm5* splicing was identified as altered by RNA-seq. *Right*, Semi-quantitative PCR of *Rbm5* isoforms using total RNA isolated from WT mESCs expressing WT or ADPRylation site mutant U2AFs differentiated for 12 hours.

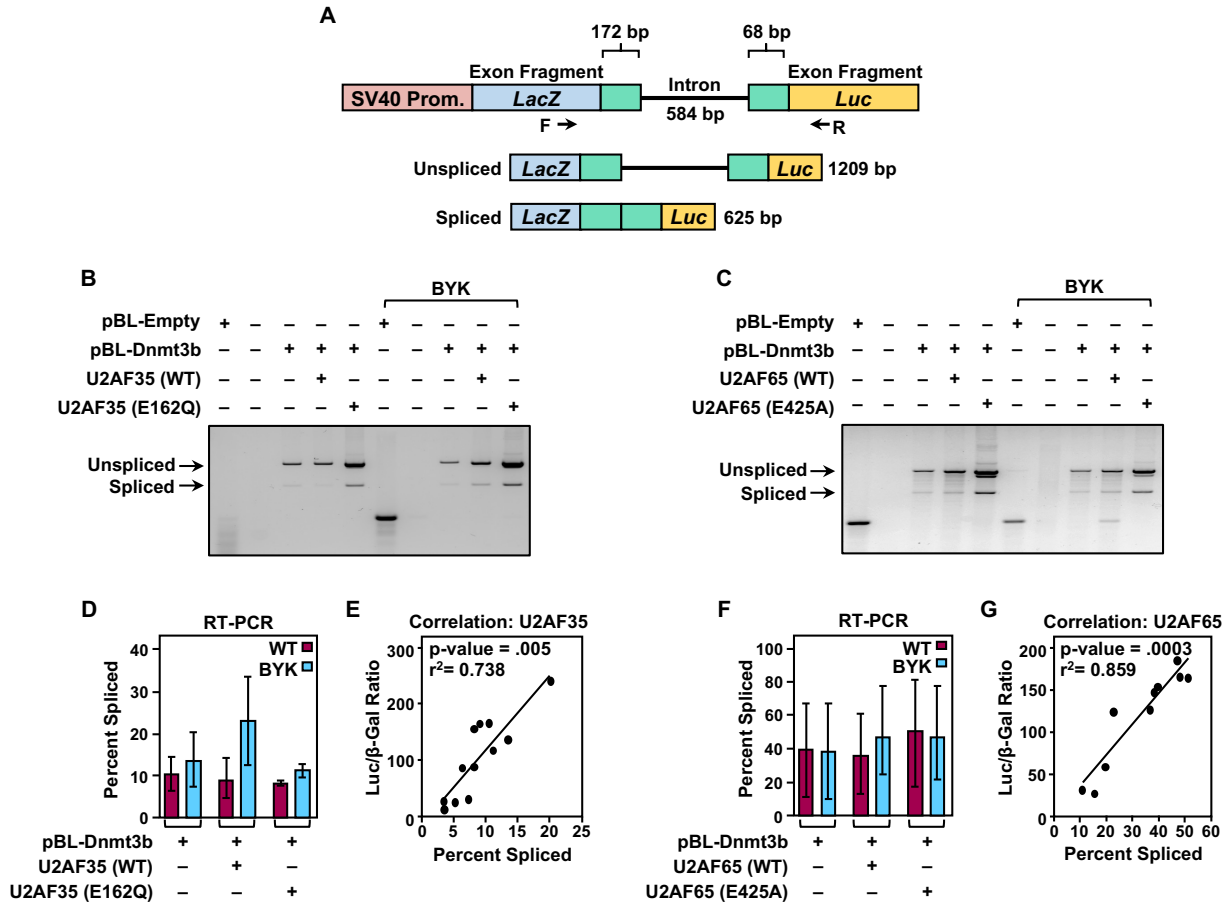

Supplemental Figure S14. Verification of the luminescence-based splicing reporter.
(A) Diagram of the pBPLUGA dual splicing reporter containing fragments of splice sites from *Dnmt3b* (U2-type splicing), including depiction of the pBPLUGA-specific primers used to amplify and distinguish between the unspliced and spliced reporter mRNAs.
(B and C) RT-PCR analysis of unspliced and spliced reporter mRNAs from the pBPLUGA-*Dnmt3b* reporter, which was electroporated into mESCs with expression vectors for WT or ADPRylation site mutant U2AF35 (B) or U2AF65 (C). The cells were treated with or without BYK204165 (BYK) as indicated. The RT-PCR products were run on 2% gels. PCR products representing unspliced and spliced products are marked with arrows.
(D-G) Quantification (D, F) and correlation with luminescence output (E, G) for assays using the pBPLUGA-*Dnmt3b* reporter. For the quantification (D, F) of assays like those shown in panels B and C, the signal from each spliced band was divided by the sum of the corresponding spliced and unspliced bands (spliced product/total PCR product). This ratio was then multiplied by 100 to yield the percent spliced. The bars in the graph represent the mean ± range (n =2). For the correlation with luminescence output (E, G), the percent splicing from the RT-PCR analyses was correlated with mean splicing efficiency ratios from the luminescence-based assays from Figure 7, B and C. ($n \geq 3$, Pearson correlation).

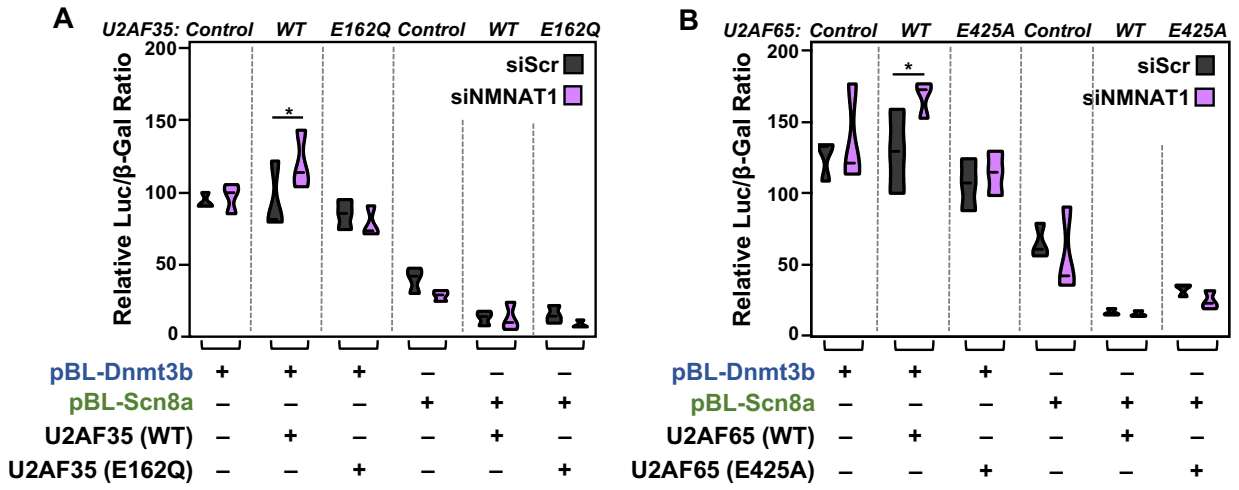

Supplemental Figure S15. Depletion of NMNAT1 alters spicing in mESCs.
(A and B) Relative luciferase/β-galactosidase activity ratios from assays in siRNA-treated WT mESCs using the *Dnmt3b* and *Scn8a* pBPLUGA reporter constructs in the presence of WT or ADPRylation site mutant U2AFs (E162Q U2AF35 and E425A U2AF65). Activity of luciferase and ß-galactosidase protein after electroporation of the reporter constructs along with plasmids encoding trans-acting factors (A) U2AF35 WT or U2AF35 E162Q or (B) U2AF65 WT or U2AF65 E425A into siScr or siNMNAT1-treated mESCs after 24 hours of differentiation. Quantification of results as violin plots (n = 3, two-way ANOVA, Fisher's LSD, $^{*}p < 0.05$, $^{**}p < 0.001$).

LEGENDS FOR SUPPLEMENTAL DATA TABLES

Supplemental Data Table S1. Metabolomic analysis of NAD^+ pathway metabolites.
Wild-type (WT) and *Parp1*$^{-/-}$ (P1KO) mESCs were differentiated for 0, 6, 12, 24, and 72 hours. The metabolites were then acid extracted and LC-MS was performed to quantify NAD^+ pathway metabolite levels. Each sheet summarizes processed and normalized metabolite levels. The "Tab" key provides details about all the other worksheets contained within this spreadsheet. The "Column Heading" key provides annotation information describing labels used in each "Tab".

Supplemental Data Table S2. Mass spectrometry results from experiments using an asPARP-1 approach in murine embryonic stem cells.
Nuclear extracts were prepared from twelve hour differentiated wild-type mouse embryonic stem (WT mESCs). The extracts were incubated with purified recombinant wtPARP1 or asPARP1 in the presence of 8-Bu(3-yne)T-NAD^+ for PARP1-specific labeling of extract proteins. The 8-Bu(3-yne)T-ADP-ribosylated proteins were then covalently linked to azide-agarose. The conjugated azido-agarose beads were washed, trypsinized to release peptides for protein identification, and then washed again. The remaining peptides containing ADP-ribosylation sites were eluted from the resin using hydroxylamine (NH_2OH) for site identification. Both the tryptic digest eluate (Peptide ID) and hydroxylamine eluate (Site ID) were subjected to LC-MS/MS analysis. Analysis was performed by 'subtracting' peptides that were identified in the wtPARP1 samples as background. The "Column Heading" key provides annotation information describing the metrics of each of the LC-MS/MS-identified peptides. The "Tab" key provides details about all the other worksheets contained within this spreadsheet.

Supplemental Data Table S3. MISO analysis of RNA-seq data for protein-coding genes (mRNA).
Wild-type (WT) and *Parp1*$^{-/-}$ (P1KO) mESCs were differentiated for 0, 6, 12, 24, and 72 hours, followed by total RNA isolation, polyA+ RNA isolation, paired-end sequencing, and alternative splicing analysis. Each sheet summarizes the compiled and filtered results for MISO analysis from both replicates of significantly altered splicing events for the comparisons listed below. Significantly altered splicing events were defined as a $\Delta PSI > 0.2$ and Bayes factor (BF) > 5. The "Tab" key provides details about all the other worksheets contained within this spreadsheet. The "Column Heading" key provides annotation information describing the metrics of the identified splicing events.

Supplemental Data Table S4. rMATS analysis of RNA-seq data for protein-coding genes (mRNA).
Wild-type (WT) and *Parp1*$^{-/-}$ (P1KO) mESCs were differentiated for 0, 6, 12, 24, and 72 hours, followed by total RNA isolation, polyA+ RNA isolation, paired-end sequencing, and alternative splicing analysis. Each sheet summarizes raw rMATS output from both replicates for the comparisons listed below. The "Tab" key provides details about all the other worksheets contained within this spreadsheet. The "Column Heading" key provides annotation information describing the metrics of the identified splicing events.

SUPPLEMENTAL MATERIALS AND METHODS

Antibodies

The custom recombinant poly(ADP-ribose) binding reagent (anti-PAR) was generated and purified in house (Gibson et al. 2017) (now available from EMD Millipore; catalog no. MABE 1016). The custom rabbit polyclonal antiserum against PARP1 was generated in-house by using a purified recombinant antigen comprising the amino-terminal half of PARP1 (Kim et al. 2004) (now available from Active Motif; catalog no. 39559). The custom rabbit polyclonal antiserum against NMNAT-1 was generated in-house using recombinant human and mouse NMNAT-1 (Ryu et al. 2018). The custom rabbit polyclonal antiserum against NMNAT-2 was generated in-house using recombinant human NMNAT-2 (Challa et al. 2021).

The other antibodies used were as follows: NANOG (Abcam, ab70482), NAMPT (SantaCruz, sc-393444), U2AF35/U2AF1 (Abcam, ab86305), U2AF65/U2AF2 (Abcam, ab37530), Actin (Cell Signaling Technology, 3700S), FLAG (Sigma-Aldrich, F3165), SNRP70 (Abcam, ab83306), rabbit IgG (ThermoFisher, 10500C), goat anti-rabbit HRP-conjugated IgG (ThermoFisher, 31460), goat anti-mouse HRP-conjugated IgG (ThermoFisher, 31430).

Cell culture

Parp1$^{+/+}$ (wild-type; WT) and *Parp1*$^{-/-}$ (knockout; P1KO) mESCs (Yang et al. 2004; Gao et al. 2009) (kindly provided by Zhao-Qi Wang, Leibniz Institute for Age Research - Fritz Lipmann Institute) were maintained on a feeder layer of CF6Neo mouse embryonic fibroblasts (ThermoFisher, A34963) in Dulbecco's modified Eagle medium (DMEM; Gibco, 11965) containing 2 mM L-glutamine (Sigma Aldrich, G7513), supplemented with 15% (v/v) fetal bovine serum (Atlanta Biologicals, S11595), 0.1 mM nonessential amino acids (Sigma Aldrich, M7145), 1 mM sodium pyruvate (Invitrogen; 11360070), 0.15% leukocyte inhibitory factor (LIF; made in-house), 1% penicillin/streptomycin (Sigma Aldrich, P0781), and 0.1% (v/v) β-mercaptoethanol (Gibco, 21985023). Feeder cells were depleted for experimental assays by two passages on 0.2% gelatin coated plates. mESCs were differentiated in ultra-low attachment plates (ThermoFisher, 05-539-101) coupled with LIF removal, unless noted that differentiation was performed solely by LIF removal.

HEK-293T cells were purchased from the American Type Cell Culture (ATCC). They were cultured in DMEM (Sigma-Aldrich, D5796) supplemented with 10% fetal bovine serum (Sigma, F88067) and 1% penicillin/streptomycin.

For both cell lines, fresh cell stocks were regularly replenished from the original stocks, verified for cell type identity using the GenePrint 24 system (Promega, B1870) or by unique genetic identifiers (e.g., *Parp1*$^{-/-}$), and confirmed as mycoplasma-free every three months using a commercial testing kit. The mESCs feeder cells were mycoplasma tested by the manufacturer.

Cell treatments

mESCs or 293T cells were grown until the desired colony density or confluence and then treated for the experiments described herein. mESCs cells were differentiated by LIF removal and by growth in ultra-low attachment plates. For splicing reporter and Western blot assays, mESCs were treated with BYK204165 (PARP1 inhibitor, 10 μM; Santa Cruz, sc-214642) for 2 hours prior to the end of the differentiation time point before collection. For NAD^+ biosensor imaging assays, the cells were treated with Veliparib (ABT-888, PARP inhibitor, 10 μM; MedChem Express, HY-10129), for 2 hours prior to the end of the differentiation time point before collection.

siRNA-mediated knockdown in WT mESCs

For siRNA-mediated knockdown of endogenous *Nmnat1*, *Qprt*, and *Nampt*, WT mESCs were transfected with the siRNAs described below (purchased from Sigma) or the control siRNA (SIC001) 24 hours prior to differentiation using Lipofectamine RNAiMAX reagent (Invitrogen, 13778150) according to the manufacturer's instructions. The cells were then differentiated as described above. The siRNA oligos used to knockdown the NAD^+ synthesis enzymes were as follows:

- *NMNAT1* (siRNA1: SASI_Mm02_00338551, siRNA2: SASI_Mm02_00338554)
- *QPRT* (siRNA1: SASI_Mm01_00195365, siRNA2: SASI_Mm01_00195368)
- *NAMPT* (siRNA1: SASI_Mm01_00149471, siRNA2: SASI_Mm01_00149470)

Molecular cloning and expression plasmid generation

cpVenus-based NAD$^+$ sensor constructs. Expression vectors for cpVenus-based nuclear and cytoplasmic NAD^+ sensors and their corresponding cpVenus-only controls were kindly provided by Drs. Michael Cohen and Richard Goodman, Vollum Institute, Oregon Health and Science University (Cambronne et al. 2016). DNA coding for the sensors or controls was amplified using the primers listed below and then cloned into the pCDH-EF1α expression vector (kindly provided by Dr. Laura Banaszynski, UT Southwestern Medical Center) using Gibson assembly.

Splicing factor expression vectors. pCDH-EF1α vectors designed for puromycin and neomycin resistance were kindly provided by Dr. Laura Banaszynski. cDNAs coding for amino-terminally FLAG tagged U2AF35 or U2AF65 were amplified from cDNA-containing vectors (Sino Biologicals, MG5A2108-CF and HG18302-UT, respectively) using the primers listed below. The amplified products were then cloned into pCDH-EF1α and pFASTBAC by Gibson cloning with *EcoRI*. Similar vectors containing cDNAs for ADPRylation site mutants of U2AF35 (E162Q) and U2AF65 (E425A) were generated by site-directed mutagenesis using Pfu Turbo DNA polymerase (Agilent, 600250) with the primers listed below.

β-Galactosidase and luciferase dual reporter splicing assay. The pBPLUGA splicing reporter vector was kindly provided by Dr. John McCarthy, The University of Warwick (Kollmus et al. 1996). Genomic DNA to prepare the *Dnmt3b* and *Scn8a* splicing constructs was prepared with One-4-All genomic DNA miniprep kit (BioBasic, BS88504) according to the manufacturer's protocol. DNA covering the relevant intron/exon boundaries of *Dnmt3b* and *Scn8a* were amplified from genomic DNA prepared with the primers listed below. The amplified products were then cloned into pBPLUGA using ligation cloning with *SalI* and *BamHI* restriction enzymes.

Cloning primers

• ***cpVenus-based NAD$^+$ sensors***

- Nuclear sensor to pCDH-EF1α/forward
  5'-GACCGGCGCCTACTCTAGAGATGACCGGTCCAAAGAAGAA-3'
- Cytosolic sensor to pCDH-EF1α/forward
  5'-GACCGGCGCCTACTCTAGAGATGACCGGTCTGCAGAAAAA-3'
- NAD sensor to pCDH-EF1α/reverse
  5'-ATTCGAATTCGCTATTAACCTACACGTTGTGTC-3'
- cpVenus control to pCDH-EF1α/reverse
  5'-ATTCGAATTCGCTAGTTAGTTGTACTCAAGCTTGTGCCCC-3'

• ***Splicing factors***

- U2AF35 to pFASTBAC/forward
  5'-ATCCCGGTCCGAAGCGCGCGGATGGCGGAATACTT-3'
- U2AF35 to pFASTBAC/reverse
  5'-CGACGTAGGCCTTTGAATTTTACTTATCGTCGTCATCC-3'
- U2AF65 to pFASTBAC/forward
  5'-GTCCGAAGCGCGCGGATGGACTACAAGGATGACGATGACAAGATGTCGGACTTCGACGA-3'
- U2AF65 to pFASTBAC/reverse
  5'-TAGGCCTTTGAATTCTACCAGAAGTCCCG-3'
- U2AF35 to pCDH-EF1α/forward
  5'-GCCTACTCTAGAGCTAGCGATGGCGGAATACTTGGCCT-3'
- U2AF35 to pCDH-EF1α/reverse
  5'-CCGATTTAAATTCGAATTTTACTTATCGTCGTCATCC-3'
- U2AF65 to pCDH-EF1α/forward
  5'-CTCTAGAGCTAGCGATGGACTACAAGGATGACGATGACAAGATGTCGGACTTCGACGA-3'
- U2AF65 to pCDH EF1α/reverse
  5'-ATTTAAATTCGAATTCTACCAGAAGTCCCGG-3'
- U2AF35 E162Q/forward 5'-CAGTATGAAATGGGACAGTGCACAAGAGGGG-3'
- U2AF35 E162Q/reverse 5'-CCCCTCTTGTGCACGCTCCCATTTCATACTG-3'
- U2AF65 E425A/forward 5'-GACGGCGTCGCGGTGCCC-3'
- U2AF65 E425A/reverse 5'-GGGCACCGCGACGCCGTC-3'

• ***Intron/exon boundaries of Dnmt3b and Scn8a***

- Dnmt3b Exon 1/forward 5'-AACGTCGACTAATGAAGGGAGACAGCA-3'
- Dnmt3b Exon 2/reverse 5'-ATGGATCCCTGCGTGTAATTCAG-3'
- Scn8a Exon 2/forward 5'-GGCGTCGACTAACTTTTGTAGTA-3'
- Scn8a Exon 3/reverse 5'-TACGGATCCCACATTCTTGGACC-3'

Generation of mESCs with ectopic expression of proteins

Stable ectopic protein expression in WT mESCs. Lentiviruses were generated by transfecting the pCDH vectors described above into 293T cells together with the expression vectors for the VSV-G envelope protein (pCMV-VSV-G, Addgene plasmid no. 8454), the expression vector for GAG-Pol-Rev (psPAX2, Addgene plasmid no. 12260), and a vector to aid with translation initiation (pAdVAntage, Promega) using Lipofectamine 3000 transfection reagent (Thermo Fisher Scientific, L3000015) according to the manufacturer's instructions. The viruses were collected in the culture medium, concentrated by using a Lenti-X concentrator (Clontech, 631231), and used to infect mESC cells. The infected mESCs were treated with 250 μg/mL neomycin to select cells expressing wild-type and E162Q U2AF35. Lentivirus-infected mESCs were treated with 1 μg/mL puromycin to select cells expressing wild-type and E425A U2AF65. Ectopic expression of the cognate proteins was confirmed by Western blotting, followed by expansion, aliquoting, and freezing of the cells.

Transient ectopic protein expression in WT and PARP1 KO mESCs. For fluorescent NAD^+ determinations, 2 x 10^6 mESCs were transfected with the cpVenus NAD^+ sensors or corresponding control plasmids as described below using Lipofectamine 3000 transfection reagent (Thermo Fisher Scientific, L3000015) according to the manufacturer's instructions. All

experiments were performed 48 hours after transfection. For splicing assays, 2 x 10^5 mESCs were electroporated with 2 µg the pBPLUGA-Dntm3b or Scn8a vectors alone or with 2 µg of the pCDH-EF1α-U2AF35(WT)/U2AF65(WT) or U2AF35(E162Q)/U2AF65(E425A) vectors as described below using the Neon transfection system (Thermo Fisher) with the following settings: 1400 V, 10 ms pulse width, and 3 pulses. All experiments were performed within 72 hours of electroporation.

Preparation of cell extracts and Western blotting

WT and P1KO mESCs were cultured and differentiated as described above. The cells were then collected and flash frozen. For sample preparation, the cells were thawed on ice, washed twice with ice-cold phosphate-buffered saline (PBS), and lysed in Lysis Buffer [20 mM HEPES; pH 7.6, 1.5mM $MgCl_2$, 0.42 mM NaCl, 0.2mM EDTA, 25% glycerol, 500 nM APD-HPD (Sigma A0627; a PARG inhibitor preventing PAR degradation), 10 µM PJ34 (Enzo, ALX-270; a PARP1 inhibitor), 1mM DTT, 1x Protease Inhibitor Cocktail (Roche, 11697498001). The lysates were mixed gently at 4ºC for 20 minutes then clarified by centrifugation. The supernatants were transferred to fresh tubes. Protein concentrations were determined by Protein Assay Dye Reagent (BioRad, 500-0006).

For Western blotting, volumes of cell extract containing equivalent amounts of total protein, or individual in vitro PARylation reactions (see below), were run on polyacrylamide-SDS gels (10% for PAR, PARP1, NAMPT, NANOG, SNRP70; 12% for NMNAT1, NMNAT2) and transferred to a nylon-backed nitrocellulose membrane. The membranes were blocked with 5% non-fat milk dissolved in Tris-buffered saline containing 0.1% Tween 20 (TBST), incubated with the primary antibodies described above in 2% non-fat milk in TBST, and then incubated with anti-rabbit HRP-conjugated IgG (1:5000) or anti-mouse HRP-conjugated IgG (1:5000). Western blot signals were detected using an ECL detection reagent (Thermo Fisher, 34077, 34095) and a ChemiDoc Imaging System (Bio-Rad Laboratories). Western blot analysis and quantification was performed using Image Lab version 6.1 (Bio-Rad Laboratories) lane detection and band selection.

Determination of nuclear and cytoplasmic NAD^+ levels using cpVenus-based sensors

Transfection and cell culture. mESCs expressing nuclear or cytoplasmic NAD^+ sensors or their corresponding cpVenus-only controls (Cambronne et al. 2016) were used to determine changes in subcellular NAD^+ levels during differentiation as described previously (Ryu et al. 2018). mESCs were transfected with the pCDH-based plasmids for cpVenus or the NAD^+ sensors described in using Lipofectamine 3000 according to the manufacturer's instructions. Twenty-four hours later, the cells were trypsinized and plated in 8-well glass bottom chamber slides (Thermo Fisher, 15411) in cell culture medium. The cells were differentiated solely by LIF removal as indicated before imaging.

Imaging to determine sensor activity. Immediately before microscopy, the medium was replaced with Fluorobrite medium (Thermo Fisher, A1896701) supplemented with 15% fetal bovine serum (Atlanta Biologicals; S11595) with or without LIF for the times indicated. Representative live-cell images were taken at 63x magnification on a Zeiss LSM 880 confocal microscope affixed with a 37°C, 5% CO_2 incubator as previously described (Ryu et al. 2018). For quantification of the relative NAD^+ levels, the cells were treated as described above and the confocal images were acquired with tile scan at 20x magnification. The ratios of fluorescence intensities were determined at 488 nm to 405 nm of the sensors and the cpVenus controls for three independent biological replicates for each condition.

Image analysis and quantification of relative NAD$^+$ levels. We used Fiji ImageJ software to subtract background, set thresholds, select the regions of interest (ROIs), quantify NAD$^+$ levels via ratiometric fluorescent intensity, and generate TIFF images. To generate pixel-by-pixel ratiometric images, we used a custom MATLAB script described previously (Ryu et al. 2018). Ratiometric analyses (488/405 nm) of the sensor versus cpVenus controls were used to normalize sensor expression levels and to analyze the changes in subcellular NAD$^+$ levels. Average ratiometric values for the undifferentiated cpVenus-transfected mESC cells were set to 1 and the rest of the data were normalized accordingly.

Quantification of NAD$^+$-related metabolites using mass spectrometry

Collection of samples for mass spectrometry-based metabolomics. mESCs were seeded at 1.5 x 10^6, cultured, and differentiated as described above. Cells from suspension plates were collected by brief, gentle centrifugation, rinsed quickly with ice-cold saline solution, and frozen on dry ice. Then 500 µL of 80% (v/v) acetonitrile chilled to -20°C was added to the microfuge tube, which was capped and placed immediately in liquid nitrogen. The cells were subjected to cycles of three freeze-thaw lyses alternating between liquid nitrogen and 37°C. The lysed cells were then centrifuged at 20,000 x g for 15 minutes at 4°C. The metabolite-containing supernatant was transferred to a new tube and stored at -80°C until analyzed by mass spectrometry.

Running the samples and collecting mass spectra. For targeted metabolomic analysis, the metabolite-containing supernatants from mESCs described above were reconstituted in 100 µL of 80% acetonitrile/20% water and then analyzed with a SCIEX QTRAP 5500 liquid chromatograph/triple quadrupole mass spectrometer. Most metabolites were analyzed using a Nexera Ultra-High-Performance Liquid Chromatograph system (Shimadzu Corporation) with a SeQuant® ZIC®-pHILIC HPLC column (150 × 2.1 mm, 5 µm, polymeric) at 35°C (nicotinate was the exception; see below). The mass spectrometer was used with an electrospray ionization (ESI) source in multiple reaction monitoring (MRM) mode. The composition of mobile phase A was 10 mM ammonium acetate in water (pH 9.8 adjusted with ammonium water) and the composition of mobile phase B was 100% acetonitrile. The elution gradient was 0-15 minutes, linear gradient 90-30% B, then the column was washed with 30% B for 4 minutes before reconditioning it for 6 minutes using 90% B. The flow rate was 0.25 mL/minute and the injection volume was 20 µL. We acquired MRM data with Analyst 1.6.3 software (SCIEX). The MRM used for metabolites were adenine (Q1/Q3: 136/65, CE: 45); NAD$^+$ (Q1/Q3: 664/428, CE: 35); nicotinamide riboside (Q1/Q3: 255/78, CE: 57) or (Q1/Q3: 255/123, CE: 15); quinolinate (Q1/Q3: 168/150, CE: 13); NAAD (Q1/Q3: 665/542, CE: 20); glutamine (Q1/Q3: 147/84, CE: 23); L-kynurenine (Q1/Q3: 209/192, CE: 12); tryptophan (Q1/Q3: 205/91, CE: 51) or (Q1/Q3: 205/188, CE: 13); nicotinamide mononucleotide (Q1/Q3: 335/123, CE: 30) or (Q1/Q3: 335/97, CE: 35); nicotinamide (Q1/Q3: 123/78, CE: 29); nicotinic acid mononucleotide (Q1/Q3: 336/124, CE: 18); N-formyl-kynurenine (Q1/Q3: 237/202, CE: 11) or (Q1/Q3: 237/192, CE: 15); 3-OH-kynurenine (Q1/Q3: 225/190, CE: 22) or (Q1/Q3: 225/110, CE: 21); and ATP (Q1/Q3: 506/159, CE: -38) or (Q1/Q3: 506/79, CE: -112).

For nicotinate, we used a Phenomenex Synergi Polar-RP HPLC column (150 × 2 mm, 4 µm, 80 Å) at 35°C. The elution gradient was: 0-3 minutes, 0% B, followed by a linear gradient in 3-15 minutes, 0-100% B, then the column was washed with 100% B for 2 minutes before reconditioning it for 4 minutes using 0% B. The flow rate was 0.5 mL/minute and the injection volume was 20 µL. The MRM used for nicotinate was Q1/Q3 (124/78, CE: 29).

Analysis of the metabolomic data. The peak values assigned to each metabolite in each sample per replicate were normalized to the cell count for that replicate. The values from the 6 hour and 12 hour time points were averaged together to reduce the noise from these temporally related collections, which exhibited the greatest biological variability. Then, the fold change value was calculated relative to each cell type (WT or P1KO) at the 0 hour time point. Additionally, the fold change value was calculated between cell type (WT and P1KO) at each respective time point. Statistical significance was calculated using a 2-way ANOVA/Tukey's multiple comparison test. This test is appropriate for determining whether the means of two populations derived from a time course are equal. These analyses were verified using MetaboAnalyst (Pang et al. 2021), which was used to determined statistical significance with both ANOVA and multivariate empirical Bayes statistics (MEBA).

Expression and purification of recombinant proteins

We used Sf9 insect cells to express and purify PARP1, asPARP1, and wild-type and mutant U2AF35 and U2AF65 as described previously (Gibson et al. 2016; Gibson et al. 2017). Sf9 cells were cultured in SF-II 900 medium (Invitrogen) and transfected with 1 μg of bacmid driving expression of the following: (1) FLAG-tagged wild-type or NAD^+ analog-sensitive (L877A) mouse PARP1, (2) FLAG-tagged wild-type or ADPRylation site mutant (E162Q) mouse U2AF35, or (3) FLAG-tagged wild-type or ADPRylation site mutant (E425A) mouse U2AF65 using Cellfectin transfection reagent (Invitrogen) as described by manufacturer. After 5 hours, the medium was supplemented with 10% FBS, penicillin, and streptomycin. After three days, the medium was collected as the initial baculovirus stock. After multiple rounds of amplification, the resulting high titer baculovirus was used to infect fresh suspension cultures of Sf9 cells to induce expression of protein for two days. The protein-expressing Sf9 cells were collected by centrifugation, flash frozen in liquid nitrogen, and stored at -80°C.

For purification of the recombinant proteins, the Sf9 cell pellets were thawed on ice, resuspended in FLAG Lysis buffer (20 mM HEPES pH 7.9, 500 mM NaCl, 4 mM $MgCl_2$, 0.4 mM EDTA, 20% glycerol, 250 mM nicotinamide, 2 mM β-mercaptoethanol, and 2x protease inhibitor cocktail) and lysed by Dounce homogenization (Wheaton). The lysates were clarified by centrifugation (15,000 rpm, 30 minutes, 4°C), diluted with equal parts FLAG Dilution Buffer (20 mM HEPES pH 7.9, 10% glycerol, 0.02% NP-40), and sonicated (15 seconds, 65% amplitude) and then clarified again by centrifugation. M2 anti-FLAG agarose resin (Sigma, A2220) was added to the supernatants and incubated for three hours. The resin was washed twice with FLAG Wash Buffer 1 (20 mM HEPES pH 7.9, 150 mM NaCl, 2 mM $MgCl_2$, 0.2 mM EDTA, 15% glycerol, 0.01% NP-40, 50 mM nicotinamide, 0.2 mM β-mercaptoethanol, 1 mM PMSF, 1 μM aprotinin, 100 μM leupeptin), twice with FLAG Wash Buffer 2 (20 mM HEPES pH 7.9, 1 M NaCl, 2 mM $MgCl_2$, 0.2 mM EDTA, 15% glycerol, 0.01% NP-40, 50 mM nicotinamide, 0.2 mM β-mercaptoethanol, 1 mM PMSF, 1 μM aprotinin, 100 μM leupeptin), and twice with FLAG Wash Buffer 3 (20 mM HEPES pH 7.9, 150 mM NaCl, 2 mM $MgCl_2$, 0.2 mM EDTA, 15% glycerol, 0.01% NP-40, 0.2 mM β -mercaptoethanol, 1 mM PMSF, 1 μM aprotinin, 100 μM leupeptin). Note that the high salt Wash Buffer 2 was used to remove nucleic acids from PARP1 and the splicing factors (Kim et al. 2004). After washing, the resin was transferred to new tube for elution of the FLAG-tagged recombinant proteins using FLAG Wash Buffer 3 containing 0.5 mg/mL 3xFLAG peptide (Sigma, F4799). The eluted proteins were aliquoted and flash frozen in liquid nitrogen. Quality assessment and determination of the concentrations of the purified proteins were

performed by SDS-PAGE analysis versus BSA protein standards followed by staining with Coomassie Brilliant Blue.

Identification of PARP1 substrates using an NAD^+ analog-sensitive PARP1 (asPARP1) approach

We used an NAD^+ analog-sensitive PARP1 (asPARP1) approach coupled with protein mass spectrometry as described previously (Gibson et al. 2016; Gibson et al. 2017) to identify protein substrates of PARP1 catalytic activity, as well as the specific amino acid residues modified by PARP1 in those substrates. First, we verified the system using in vitro enzyme assays and in-gel fluorescence assays. Then, we used the asPARP1 approach with cell extract from WT mESC cells at 12 hours of differentiation, followed by mass spectrometry to identify the ADPRylated proteins and the specific sites of modification.

In-gel fluorescence to test asPARP1-specific modification of nuclear extract proteins. Nuclear extracts were prepared from WT mESC cells at 12 hours of differentiation as described previously (Gibson et al. 2016; Gibson et al. 2017). One μg of purified PARP1 protein (wild-type or analog-sensitive) was incubated with 50 μg of WT mESC cell nuclear extract and 250 μM of 8-Bu(3-yne)T-NAD^+ (BIOLOG Life Science Institute, Germany) for 15 minutes at room temperature. The reactions were stopped by methanol:chloroform precipitation. After centrifugation for 10 minutes at maximum speed in a microfuge at room temperature, the protein pellets were dissolved in 1 mL of Urea Solubilization Buffer (200 mM HEPES pH 8.0, 8 M urea, 1 M NaCl, 4% CHAPS). Fifty μL from the 1 mL of labeled and solubilized proteins were combined sequentially in the following order with mixing: 1 μL azido-TAMRA (Click Chemistry Tools), 2 μL of a 50:250 mM CuSO4:THPTA pre-formed catalytic complex, 1 μL of 500 mM aminoguanidine hydrochloride, and 1 μL of 500 mM sodium ascorbate. After incubation in the dark for 2 h, the fluorescently labeled PARP1 target proteins were extracted by methanol:chloroform precipitation, run on an SDS-PAGE gel, and visualized using a Bio-Rad Pharos FX Plus Molecular Imager.

Large scale labeling of nuclear extract proteins using asPARP1. Nuclear extracts prepared from differentiated WT mESC were prepared as described above. Twenty μg of PARP1 or asPARP1 protein were combined with PARP1 Reaction Buffer (30 mM HEPES, pH 8.0, 5 mM $MgCl_2$, 5mM $CaCl_2$, 0.01% NP-40, 100 μg/mL bovine serum albumin, 1 mM DTT, protease inhibitors, and phosphatase inhibitors) containing 100 μg/mL freshly added sonicated salmon sperm DNA (sssDNA) and incubated for 5 minutes at room temperature. One mg of room temperature WT mESC nuclear extract was added to the reaction and incubated with gentle mixing for 5 minutes. Two hundred and fifty μM of room temperature 8-Bu(3-yne)T-NAD^+ was added to the mixture and incubated for 15 min with continuous gentle mixing. The reaction was terminated by methanol:chloroform precipitation.

Preparation of the samples for LC-MS/MS. Following the ADPRylation reaction, the precipitated protein pellet was collected and resuspended in Urea Solubilization Buffer (200 mM HEPES pH 8.0, 8 M urea, 1 M NaCl, 4% CHAPS) containing 250 U/mL of Universal nuclease (Pierce/Thermo). The 8-Bu(3-yne)T-ADPRylated nuclear proteins in Urea Solubilization Buffer were combined sequentially in a 2 mL tube in the following order with mixing: 100 μL azido-agarose beads (Click Chemistry Tools), 820 μL water, 40 μL of a 50:250 mM CuSO4:THPTA pre-formed catalytic complex, 20 μL of 500 mM aminoguanidine hydrochloride, and 20 μL of 500 mM sodium ascorbate. After 18 hours of click chemistry reaction time in the dark with slow mixing in a rotating mixer, the beads were collected by centrifugation at room temperature for 1

minute at 1,000 RCF in a microcentrifuge and the reaction supernatant was aspirated. The beads were resuspended in 1.8 mL of MilliQ water and were collected by centrifugation at room temperature for 1 minute at 1,000 RCF. The beads were then resuspended in 1 mL of SDS Wash Buffer (100 mM Tris·HCl pH 8.0, 1% SDS, 250 mM NaCl, 5 mM EDTA) supplemented with freshly made 1 mM DTT, heated to 70°C for 15 minutes, and then allowed to cool to room temperature.

The beads were collected by centrifugation at room temperature for 5 minutes at 1000 x g in a microcentrifuge and the supernatant was aspirated. The beads were then resuspended in 1 mL of SDS Wash Buffer containing 40 mM iodoacetamide and incubated at room temperature for 30 minutes in the dark to alkylate the cysteine residues. The beads were then transferred to a 2 mL single-use column (Bio-Rad) and washed as follows: 10 washes of 2 mL each with SDS Wash Buffer, 10 washes of 2 mL each with Urea Wash Buffer (100 mM Tris·HCl pH 8.0, 8 M urea), and 10 washes of 2 mL each with 20% acetonitrile.

Following the extensive washing, the beads were resuspended in 500 µL of Trypsin Digestion Buffer (100 mM Tris·HCl pH 8.0, 2 mM $CaCl^2$, 10% acetonitrile). Trypsin digestion of the bead-bound 8-Bu(3-yne)T-ADPRylated nuclear extract proteins was performed by addition of 1 µg of trypsin (Promega) to the Trypsin Digestion Buffer, with incubation at room temperature overnight with slow mixing on a rotating mixer. The peptides from the trypsin digestion were prepared for LC MS/MS by desalting on a C18 stage tip (Thermo) according to the manufacturer's protocol and lyophilized for storage at -80°C prior to the LC-MS/MS runs for peptide identification.

After the trypsin digestion of the proteins on the beads, which left the peptides covalently linked to the beads through the azide-clicked 8-Bu(3-yne)T-ADPRylation sites, the beads were transferred to a fresh 2 mL single use column (Bio-Rad) and washed as follows: 10 washes of 2 mL each with SDS Wash Buffer, 10 washes of 2 mL each with Urea Wash Buffer, 10 washes of 2 mL each with 20% acetonitrile, and 5 washes of 2 mL each with Peptide Elution Buffer (100 mM HEPES, pH 8.5). The beads were transferred to a microcentrifuge tube and hydroxylamine (Sigma) was added to 0.5 M to elute the glutamate- and aspartate-modified 8-Bu(3-yne)T-ADPRylated peptides from the beads. The eluted peptides were prepared for LC-MS/MS by desalting on a C18 stage tip (Thermo) according to the manufacturer's protocol and then lyophilized for storage at -80°C prior to LC-MS/MS analysis.

LC-MS/MS analysis. Following solid-phase extraction cleanup with an Oasis HLB microelution plate (Waters), the trypsin samples were reconstituted in 2% (v/v) acetonitrile (ACN) and 0.1% trifluoroacetic acid in water such that the resulting concentration was 1 µg/µL. The hydroxylamine-eluted samples were reconstituted in 6 µL of the same buffer. One µL of the trypsin-digested samples and 5 µL of the hydroxylamine-eluted samples were injected onto an Orbitrap Fusion Lumos mass spectrometer (Thermo Electron) coupled to an Ultimate 3000 RSLC-Nano liquid chromatography system (Dionex). Samples were injected onto a 75 µm i.d., 50-cm long EasySpray column (Thermo) and eluted with a gradient from 1%-28% Buffer B over 60 minutes. Buffer A contained 2% (v/v) acetonitrile and 0.1% formic acid in water, and Buffer B contained 80% (v/v) acetonitrile, 10% (v/v) trifluoroethanol, and 0.1% formic acid in water.

The mass spectrometer was operated in positive ion mode with a source voltage of 1.5-2.4 kV and an ion transfer tube temperature of 275°C. MS scans were acquired at a resolution of 120,000 in the Orbitrap and up to 10 MS/MS spectra were obtained in the ion trap for each full spectrum acquired using higher-energy collisional dissociation (HCD) for ions with charges 2-7. Dynamic exclusion was set for 25 s after an ion was selected for fragmentation. Raw MS data

files were analyzed using Proteome Discoverer v2.2 (Thermo), with peptide identification performed using Sequest HT searching against the *Mus musculus* database from UniProt. Fragment and precursor tolerances of 10 ppm and 0.6 Da were specified, and three missed cleavages were allowed. Carbamidomethylation of Cys was set as a fixed modification, with oxidation of Met and hydroxamic acid addition (+15.0109 Da) to Asp and Glu set as variable modifications. The false-discovery rate (FDR) cutoff was 1% for all proteins and peptides.

Defining the high confidence universe. Peptides identified from samples prepared with wild-type PARP1 (wtPARP1) were treated as non-specific background. To be considered as a high confidence PARP1 ADPRylation substrate, the protein was either not identified or was found at a ≥15-fold less abundance in the wtPARP1 sample compared to the asPARP1 sample. In addition, the protein had to be identified in at least two of the three replicates.

Structural Analysis of U2AF35

The crystal structure of the yeast homolog of U2AF1 (U2AF35) bound to 3' splice site RNA was downloaded from the Research Collaboratory for Structural Bioinformatics Protein Data Bank (RCSB PDB) using PDB ID 7c06.6 (Yoshida et al. 2020). The predicted structure of mouse U2AF35 was downloaded from AlphaFold Protein Structure Database using ID: AF-Q9D883-F1 (Jumper et al. 2021). Both structures were uploaded, overlaid, positioned, and colorized using PyMOL.

RNA isolation and PCR-based gene expression and splicing assays

RNA isolation. WT and P1KO ESCs were plated, grown, and differentiated as described above. The cells were collected at the indicated time points and total RNA was isolated using an RNeasy Plus Mini Kit (Qiagen) according to the manufacturer's protocol. Total RNA was reverse transcribed using oligo(dT) primers or random hexamers (for downstream use in semi-quantitative PCR) plus MMLV reverse transcriptase (Promega) to generate cDNA pools.

Reverse transcription-quantitative PCR (RT-qPCR). The cDNA pools were subjected to qPCR using the gene-specific primers listed below as described previously (Liu and Kraus 2017). Briefly, cDNA, 1x SYBR Green PCR master mix, and the forward and reverse primers (250 nM) were mixed and subjected to 45 cycles of amplification (95°C for 10 s, 60°C for 10 s, 72°C for 1 s) following an initial 5 minute incubation at 95°C using a Roche LightCycler 480 384-well qPCR system. Melting curve analyses were performed to ensure that only the targeted amplicon was amplified. Target gene expression was normalized to the expression of *Gapdh* mRNA (mouse). Relative expression was determined in comparison to the value of an appropriate control sample. All experiments were performed at least three times with independent biological replicates to ensure reproducibility. All experimental groups that were compared had similar variance as determined by the standard deviation of the biological replicates within each group. Statistical differences between two groups were determined using the Student's t test and a statistical significance was defined as $p < 0.05$.

Reverse transcription-semiquantitative PCR (RT-sqPCR). The cDNA samples were subjected to PCR using the isoform-specific primers listed below, as described previously (Harvey et al. 2021). Briefly, cDNA, 250 μM dNTP (Fisher, 50-305-950), and 0.25 μM forward and reverse primers, and 0.15 μL XL Taq (prepared in-house) were mixed with 10x Thermopol Buffer (NEB, B9004S) and then amplified for primer pair-specific optimized cycle numbers. The products were run on a 2% agarose gel and stained with Sybr Safe (ThermoFisher, S33102) for visualization.

Determination of luminescence-based reporter assay splicing efficiency by RT-sqPCR analysis. For determining the efficiency of splicing in the luminescence-based reporter assay (see below) by RT-sqPCR analysis, cDNA samples were generated as described above and subjected to PCR using the pBPLUGA-specific primers listed below, as described previously (Eperon et al. 2006). Briefly, cDNA, 1% DMSO (Agilent,600677),160 µM dNTP (Fisher, 50-305-950), 0.25 µM forward and reverse primers, and 1.0 µL Herculase II Fusion Polymerase (Agilent, 600677) were mixed with 5x Herculase II Reaction Buffer (Agilent, 600677) and then amplified for 24 cycles. The products were run on a 2% agarose gel and stained with Sybr Safe (ThermoFisher, S33102) for visualization. Agarose gel analysis and quantification was performed using Image Lab version 6.1 (Bio-Rad Laboratories) lane detection and band selection.

RT-PCR primers

• ***Primers for RT-qPCR***

- *Nanog*/forward	5'-CACCCACCCATGCTAGTCTT-3'
- *Nanog*/reverse	5'-ACCCTCAAACTCCTGGTCCT-3'
- *Sox2*/forward	5'-CCGTTTTCGTGGTCTTGTTT-3'
- *Sox2*/reverse	5'-TCAACCTGCATGGACATTTT-3'
- *Oct4*/forward	5'-CCAGAAGGGCAAAAGATCAA-3'
- *Oct4*/reverse	5'-CTGGGAAAGGTGTCCCTGTA-3'
- *Parp1*/forward	5'-TGTTTGCCTCTTGTGGTGAG-3'
- *Parp1*/reverse	5'-AGCGTTCCTTCCTTTGGTCT-3'
- *Pax6*/forward	5'-GGCGGTTAGAAGCACTTCAC-3'
- *Pax6*/reverse	5'-TACGCAAAGGTCCTTGGTTC-3'
- *Hand1*/forward	5'-CCCTCTTCCGTCCTCTTACC-3'
- *Hand1*/reverse	5'-ATTCAGCAACGAATGGGAAC-3'
- *Gdf1*/forward	5'-CCATCTCCGTGCTCTTCTTC-3'
- *Gdf1*/reverse	5'-TCCACCACCATGTCTTCGTA-3'
- *Krt8*/forward	5'-ACTCACTAGCCCTGGCTTCA-3'
- *Krt8*/reverse	5'-TCTTCACAACCACAGCCTTG-3'
- *Wnt8a*/forward	5'-TGCCTAGTTGCAGGACAGTG-3'
- *Wnt8a*/reverse	5'-CTACAGGCCAACCCTGTGAT-3'
- *Nmnat1*/forward	5'-TTCAAGGCCTGACAACATCGC-3'
- *Nmnat1*/reverse	5'-GAGCACCTTCACAGTCTCCACC-3'
- *Qprt*/forward	5'-GGTCAGCATTCCCAACGAGA-3'
- *Qprt*/reverse	5'-TAAAGCCAGATTCCCCAGCG-3'
- *Nampt*/forward	5'-TGGGAAGGTGACAAAAAGCTACT-3'
- *Nampt*/reverse	5'-ACATAACAACCCGGCCACAT-3'
- *Gapdh*/forward	5'-CACTGAGCATCTCCCTCACA-3'
- *Gapdh*/reverse	5'-GTGGGTGCAGCGAACTTTAT-3'

• ***Primers for RT-sqPCR***

- *Ctnnd1* Iso 1/forward	5'-AGATCAGTTTGTCACCACCC-3'
- *Ctnnd1* Iso 1/reverse	5'-TCTCTCAAGGTCAGCATCG-3'
- *Ctnnd1* Iso 2/forward	5'-CTAAACAATGCATCTAGAAGCC-3'
- *Ctnnd1* Iso 2/reverse	5'-TCAGCCTGGCAGTTGGCACAAT-3'
- *Irf9* exon1/forward	5'- TTGCCCTGCAACTCAGA-3'
- *Irf9* exon3/reverse	5'- TTGAATATGGCAGCATC-3'

- *Rbm5* exon6/forward 5'-GTGTAAGCCGTGGTTT-3'
- *Rbm5* exon9/reverse 5'-CACAGTAGTAATCCACGG-3'
- *pBPLUGA Gal3301*/forward 5'-AACATCAGCCGCTACAGTCAA-3'
- *pBPLUGA Luc3700*/reverse 5'-ACGTGATGTTCACCTCGATAT-3'

RNA-sequencing (RNA-seq)

The following methods were used to generate, evaluate for QC, sequence, and analyze the data from RNA-seq libraries.

Generation of RNA-seq libraries. Two biological replicates of WT and P1KO mESCs were plated, grown, and differentiated as described above. Total RNA was isolated using an RNeasy kit (Qiagen) according to the manufacturer's instructions. The total RNA was then enriched for polyA+ RNA using Dynabeads Oligo(dT)25 (Invitrogen). The polyA+ RNA was then used to generate paired-end strand-specific RNA-seq libraries as described previously (Zhong et al. 2011). The RNA-seq libraries were subjected to QC analyses (i.e., number of PCR cycles required to amplify each library, the final library yield, and the size distribution of final library DNA fragments) and sequenced using an Illumina HiSeq 2000.

Analysis of RNA-seq data for expression and splicing. The raw data were subjected to QC analyses using the FastQC tool (Andrews 2010). Reads were trimmed to remove adapter sequences and shorter reads to maximize mappability using Cutadapt version 2.5 (Martin 2011) with parameters specified for the proper adapter sequence and in a paired-read manner. The reads were then mapped to mouse genome (mm10) using the spliced reader aligner TopHat version 2.1.1 (Kim et al. 2013). The aligned reads were sorted and indexed using SamTools (Li et al. 2009) to format properly for downstream analysis.

Differential alternative splicing events were detected by integrating both replicates with rMATS version 4.1.1 (Shen et al. 2014). Default parameters were used with the exception of read type, which was set to paired, with allowance for variable read length. The detected alternative splicing events were imported, filtered, and visualized in R using the Maser package (Veiga 2021). Additionally, alternative splicing events and isoform usage were detected and filtered using MISO version 0.5.3 (Katz et al. 2010) with each replicate handled separately. Detected events were visualized using the Sashimi program (Katz et al. 2010). The significantly altered splicing events in the P1KO mESCs compared to WT mESCs at the indicated time points (PSI > 0.1, FDR = 0.05; PSI = percent spliced in) were used to identify PARP1-dependent splicing events. Additionally, significantly altered splicing events over the time course of differentiation (PSI > 0.1, FDR = 0.05) were used to identify differentiation-regulated splicing events. Heatmaps visualizing changes in PSI value were generated using Morpehus (Broad Institute).

Gene Ontology (GO) Analyses

Gene ontology analyses were performed using DAVID (Database for Annotation, Visualization, and Integrated Discovery) (Huang da et al. 2009b; Huang da et al. 2009a). Inputs for the GO analyses were data from the proteomic studies filtered for high confidence proteomic hits. DAVID returns clusters of related ontological terms that are ranked according to an enrichment score. The top GO biological process terms from these clusters based on the enrichment score were listed.

In vitro ADPRylation assays

In vitro PARylation assays were performed as described previously (Zhang et al. 2012; Lin et al. 2018). The reactions contained 0.1 μM purified PARP1, NAD^+, a purified protein substrate, and polypyrimidine tract RNA (sequences listed below). U2AF35 and U2AF65 proteins were purified as described above and were included at a concentration of 1 μM and 0.5 μM, respectively, per reaction. One hundred ng/μL of sheared salmon sperm DNA (Invitrogen, AM9680) was used as an allosteric activator of PARP1 enzymatic activity. Purified proteins were mixed in PARylation Buffer (20 mM HEPES pH 7.9, 5 mM $MgCl_2$, 5 mM $CaCl_2$, 25 mM KCl, 0.01% NP-40, 1 mM DTT, 100 ng/μL sheared salmon sperm DNA), then RNA was added at 2 μM to the reaction followed by the addition of 100 μM NAD^+. The PARylation reactions were incubated at room temperature for 20 minutes and stopped by the addition of one third of a reaction volume of 4x SDS-PAGE Loading Buffer (200 mM Tris·HCl pH 6.8, 8% SDS, 40% glycerol, 4% β-mercaptoethanol, 50 mM EDTA, 0.08% bromophenol blue), followed by heating to 95°C for 5 minutes. The reaction products were then resolved on a 12% or 10% SDS-PAGE gel, transferred to a nylon-backed nitrocellulose membrane, and blotted with an anti-PAR detection reagent (EMD Millipore, MABE1031). Western blot analysis and quantification was performed using Image Lab version 6.1 (Bio-Rad Laboratories) for lane detection and band selection.

RNA electrophoretic mobility assays with U2AF65

Interactions between U2AF65 and various splice site RNAs were analyzed by RNA electrophoretic mobility assays (EMSAs). Cy5-labeled RNAs containing splice sites from the mouse *Lpl* (Fu et al. 2011) or *Scn8a* (Sharp and Burge 1997) genes were folded in Folding Buffer (25 mM HEPES pH 7.6, 12.5 mM KCl, 0.5 mM $MgCl_2$) by heating the mixture at 65°C for 5 minutes, followed by gradual cooling to room temperature, protected from light. Binding reactions were performed as described previously (Fu et al. 2011). Briefly, the reaction was assembled with the following components: purified FLAG-U2AF65(WT) or FLAG-U2AF65(E425A) (1 μM), 10 nM pre-folded Cy5-*Lpl* or Cy5-*Scn8a* splice site RNA, 0.1 mg/mL yeast tRNA (AM7119, ThermoFisher), 1 mM DTT, 5% glycerol, 1x complete protease inhibitor cocktail (05056489001, Roche), 0.02 U/mL RNase inhibitor (Y9240L, Enzymatics). The reactions were then incubated for 15 minutes at 30°C before running on a native 6% polyacrylamide gel in 1x TBE for 45 minutes at 4°C in the absence of loading dye solution (to avoid changing the salt concentration). The gel was then imaged directly using a ChemiDoc MP system (Bio-Rad). Western blot analysis and quantification was performed using Image Lab version 6.1 (Bio-Rad Laboratories) for lane detection and band selection.

For the reactions performed in the presence of PAR, the RNA folding was done as mentioned above. However, the binding reaction occurred after performing an in vitro PARylation reaction as described above. The in vitro PARylation reaction was terminated by the addition of 20 μM PJ34 (a PARP1 inhibitor). Half of the PARylation reaction volume was used in the EMSA binding reaction as described above.

Splice site RNAs

• ***In Vitro PARylation***

- Strong U2 3' Splice Site	5'-UGGUGGGUUUUUUUUCAGGAA-3'
- U12 3' Splice Site	5'- AACCCUGUCUGCUCAC-3'

• ***EMSA***

- U2 *LPL* 3' Splice Site	5'-CCUGCUUUUUUCCCUUUUAAGGCCUCGAUCCA-3'

- U12 *Scn8a* 3' Splice Site 5'- CUUAACUCCUCUCUACAGU-3'

Immunoprecipitation and interaction assays

Immunoprecipitation from mESCs. mESCs expressing FLAG-tagged wild-type or mutant (E162Q) U2AF35, FLAG-tagged wild-type or mutant (E425A) U2AF65, or parental mESCs were seeded at ~5 × 10^6 cells per 15 cm diameter plate and cultured and differentiated as described above. The cell pellet was washed with ice-cold PBS and then incubated for 30 minutes with agitation at 4°C in IP-Lysis Buffer (50 mM Tris·HCl pH 7.9, 150 mM NaCl, 0.1% SDS, 0.5% deoxycholate, 1% NP-40, 10 μM PJ34, 25 μM APD-HPD, 1x protease inhibitor cocktail). After centrifugation at 10,000 x g for 15 minutes at 4°C, the supernatant was collected and the protein concentration was determined using a Bradford assay. Five mg of whole cell extract protein was incubated with anti-FLAG M2 agarose resin (Sigma, A2220) for 4 hours at 4°C and then washed 5 times with FLAG Wash Buffer 3 (see above). The immunoprecipitated FLAG-tagged U2AF proteins were recovered from the beads by either eluting with 0.5 mg/mL 3xFLAG peptide in Elution Buffer (20 mM HEPES pH 7.5, 1 mM EDTA, 10% glycerol, 150 mM NaCl, 0.01% NP-40, with freshly added 0.4 mM PMSF, 1 mM DTT, and 1x protease inhibitor cocktail, 250 nM ADP-HPD, and 10 μM PJ34)\ or heating at 100°C for 5 minutes in 2x SDS-PAGE loading buffer. The immunoprecipitated material was subjected to Western blotting as described above.

Immunoprecipitation from HEK-293T cells. HEK-293T cells ectopically expressing FLAG-tagged wild-type or mutant (E162Q) U2AF35, FLAG-tagged wild-type or mutant (E425A) U2AF35, or parental 293T were seeded at ~5 × 10^6 cells per 15 cm diameter plate, cultured, and differentiated as described above. The cell pellet was washed with ice-cold PBS and then incubated for 30 minutes with agitation at 4ºC in IP-Lysis Buffer (see above). After centrifugation at 10,000 x g for 15 minutes at 4°C, the supernatant was collected, and the protein concentration was determined using a Bradford assay. Three mg of whole cell extract protein was incubated with anti-FLAG M2 agarose resin (Sigma, A2220) for 4 hours at 4°C, and then washed 5 times with FLAG Wash Buffer 3 (see above). The immunoprecipitated FLAG-tagged U2AF proteins were recovered from the beads by either eluting with 0.5 mg/mL 3xFLAG peptide in Elution Buffer (see above) or heating at 100°C for 5 minutes in 2x SDS-PAGE loading buffer. The immunoprecipitated material was subjected to Western blotting as described above.

Cell-based dual reporter splicing assays

Cell treatment and collection. mESCs (2 x 10^5) were electroporated with the pBPLUGA constructs containing the exon-intron-exon boundary of *Dnmt3b* or *Scn8a* alone or in combination with pCDH-U2AF35(WT), pCDH-U2AF35(E162Q), pCDH-U2AF65(WT), or pCDH-U2AF65(E425A). After electroporation, the cells were seeded on gelatin-coated 12-well plates and grown overnight. For samples with siRNA-mediated knockdown, siRNA treatment was done as described above for 24 hours prior to differentiation. Differentiation was performed solely by LIF-removal for twelve hours, and 10 μM of BYK204165 (PARP1 inhibitor; sc-214642, Santa Cruz) was added during the last 2 hours of LIF removal. Cell collection and experimentation were performed as reported previously (Nasim and Eperon 2006). Briefly, the cells were collected in TEN7.5 buffer (40 mM Tris·HCl pH 7.5, 1 mM EDTA, 150 mM NaCl) and pelleted by centrifugation at 1,000 x g at 4ºC. The cell pellets were lysed in 100 μL 1x Reporter Lysis Buffer (E1500, Promega) by agitation at 4ºC for 5 minutes. The lysates were centrifuged at 10,000 x g at 4°C and the supernatants were collected.

Luminescence readings. Twenty µL of lysate was added to black-bottomed 96-well plates in duplicate, followed by the addition of 75 µL of luciferase assay reagent (E1500, Promega). The luciferase luminescence intensities were quantified immediately by spectroscopy using a plate reader (CLARIOstar BMG Labtech) with the appropriate filter to measure Firefly luciferase luminescence. Following the readings, 75 µL of Beta-Glo reagent (E4720, Promega) was added to 20 µL of lysate and incubated for 1 hour. The β-galactosidase luminescence intensities were then quantified spectroscopy using a plate reader (CLARIOstar BMG Labtech) with the appropriate filters to measure Ultraglo luminescence. All experiments were performed at least three times with independent biological replicates to ensure reproducibility. Statistical significance was calculated using a 2-way ANOVA/ Fisher's LSD multiple comparison test.

Correlation of RT-PCR with luminescence readings. For determining the efficiency of splicing in the luminescence-based reporter assay by RT-sqPCR analysis, cDNA samples were generated as described above and subjected to PCR using pBPLUGA-specific primers (listed above). The RT-sqPCR results were correlated with the luminescence results obtained from the same experimental conditions using a simple linear regression of correlation analysis (GraphPad Prism 9.3.1).

Omics data availability

The asPARP1/ADPRylated proteome mass spectrometry data can be accessed from MassIVE (www.massive.ucsd.edu) using accession number MSV000088580. Processed data identifying ADPRylated peptides and specific sites of ADPRylation can be found in Supplemental Table S1.

The RNA-seq datasets generated for this study can be accessed from the NCBI's Gene Expression Omnibus (GEO) repository (www.ncbi.nlm.nih.gov/geo/) using accession number GSE192380. Processed data quantifying specific splicing events can be found in Supplemental Tables S2 and S3.

The metabolomics mass spectrometry data can be accessed from MassIVE (www.massive.ucsd.edu) using accession number MSV000088612. Processed data identifying specific NAD^+ metabolites and precursors can be found in Supplemental Table S4.

Supplemental References

Andrews S. 2010. FastQC: A quality control tool for high throughput sequence data [Online] version GPL v3 Babraham Bioinformatics

Broad Institute. 2021. Morpheus: Versatile matrix visualization and analysis software.

Cambronne XA, Stewart ML, Kim D, Jones-Brunette AM, Morgan RK, Farrens DL, Cohen MS, Goodman RH. 2016. Biosensor reveals multiple sources for mitochondrial NAD(+). *Science* **352**: 1474-1477.

Challa S, Khulpateea BR, Nandu T, Camacho CV, Ryu KW, Chen H, Peng Y, Lea JS, Kraus WL. 2021. Ribosome ADP-ribosylation inhibits translation and maintains proteostasis in cancers. *Cell*.

Fu Y, Masuda A, Ito M, Shinmi J, Ohno K. 2011. AG-dependent 3'-splice sites are predisposed to aberrant splicing due to a mutation at the first nucleotide of an exon. *Nucleic Acids Res* **39**: 4396-4404.

Gao F, Kwon SW, Zhao Y, Jin Y. 2009. PARP1 poly(ADP-ribosyl)ates Sox2 to control Sox2 protein levels and FGF4 expression during embryonic stem cell differentiation. *J Biol Chem* **284**: 22263-22273.

Gibson BA, Conrad LB, Huang D, Kraus WL. 2017. Generation and characterization of recombinant antibody-like ADP-ribose binding proteins. *Biochemistry* **56**: 6305-6316.

Gibson BA, Zhang Y, Jiang H, Hussey KM, Shrimp JH, Lin H, Schwede F, Yu Y, Kraus WL. 2016. Chemical genetic discovery of PARP targets reveals a role for PARP-1 in transcription elongation. *Science* **353**: 45-50.

Harvey SE, Lyu J, Cheng C. 2021. Methods for characterization of alternative RNA splicing. *Methods Mol Biol* **2372**: 209-222.

Huang da W, Sherman BT, Lempicki RA. 2009a. Bioinformatics enrichment tools: paths toward the comprehensive functional analysis of large gene lists. *Nucleic Acids Res* **37**: 1-13.

-. 2009b. Systematic and integrative analysis of large gene lists using DAVID bioinformatics resources. *Nat Protoc* **4**: 44-57.

Jumper J, Evans R, Pritzel A, Green T, Figurnov M, Ronneberger O, Tunyasuvunakool K, Bates R, Zidek A, Potapenko A et al. 2021. Highly accurate protein structure prediction with AlphaFold. *Nature*.

Katz Y, Wang ET, Airoldi EM, Burge CB. 2010. Analysis and design of RNA sequencing experiments for identifying isoform regulation. *Nat Methods* **7**: 1009-1015.

Kim D, Pertea G, Trapnell C, Pimentel H, Kelley R, Salzberg SL. 2013. TopHat2: accurate alignment of transcriptomes in the presence of insertions, deletions and gene fusions. *Genome Biol* **14**: R36.

Kim MY, Mauro S, Gevry N, Lis JT, Kraus WL. 2004. NAD+-dependent modulation of chromatin structure and transcription by nucleosome binding properties of PARP-1. *Cell* **119**: 803-814.

Kollmus H, Flohe L, McCarthy JE. 1996. Analysis of eukaryotic mRNA structures directing cotranslational incorporation of selenocysteine. *Nucleic Acids Res* **24**: 1195-1201.

Li H, Handsaker B, Wysoker A, Fennell T, Ruan J, Homer N, Marth G, Abecasis G, Durbin R, Genome Project Data Processing S. 2009. The Sequence Alignment/Map format and SAMtools. *Bioinformatics* **25**: 2078-2079.

Lin KY, Huang D, Kraus WL. 2018. Generating protein-linked and protein-free mono-, oligo-, and poly(ADP-ribose) in vitro. *Methods Mol Biol* **1813**: 91-108.

Liu Z, Kraus WL. 2017. Catalytic-independent functions of PARP-1 determine Sox2 pioneer activity at intractable genomic loci. *Mol Cell* **65**: 589-603 e589.

Martin M. 2011. Cutadapt removes adapter sequences from high-throughput sequencing reads. *2011* **17**: 3.

Nasim MT, Eperon IC. 2006. A double-reporter splicing assay for determining splicing efficiency in mammalian cells. *Nat Protoc* **1**: 1022-1028.

Pang Z, Chong J, Zhou G, de Lima Morais DA, Chang L, Barrette M, Gauthier C, Jacques PE, Li S, Xia J. 2021. MetaboAnalyst 5.0: narrowing the gap between raw spectra and functional insights. *Nucleic Acids Res* **49**: W388-W396.

Ryu KW, Nandu T, Kim J, Challa S, DeBerardinis RJ, Kraus WL. 2018. Metabolic regulation of transcription through compartmentalized NAD(+) biosynthesis. *Science* **360**.

Sharp PA, Burge CB. 1997. Classification of introns: U2-type or U12-type. *Cell* **91**: 875-879.

Shen S, Park JW, Lu ZX, Lin L, Henry MD, Wu YN, Zhou Q, Xing Y. 2014. rMATS: robust and flexible detection of differential alternative splicing from replicate RNA-Seq data. *Proc Natl Acad Sci U S A* **111**: E5593-5601.

Veiga DFT. 2021. maser: Mapping Alternative Splicing Events to pRoteins. R package version 1.8.0.

Yang YG, Cortes U, Patnaik S, Jasin M, Wang ZQ. 2004. Ablation of PARP-1 does not interfere with the repair of DNA double-strand breaks, but compromises the reactivation of stalled replication forks. *Oncogene* **23**: 3872-3882.

Yoshida H, Park SY, Sakashita G, Nariai Y, Kuwasako K, Muto Y, Urano T, Obayashi E. 2020. Elucidation of the aberrant 3' splice site selection by cancer-associated mutations on the U2AF1. *Nat Commun* **11**: 4744.

Zhang T, Berrocal JG, Yao J, DuMond ME, Krishnakumar R, Ruhl DD, Ryu KW, Gamble MJ, Kraus WL. 2012. Regulation of poly(ADP-ribose) polymerase-1-dependent gene expression through promoter-directed recruitment of a nuclear NAD+ synthase. *J Biol Chem* **287**: 12405-12416.

Zhong S, Joung JG, Zheng Y, Chen YR, Liu B, Shao Y, Xiang JZ, Fei Z, Giovannoni JJ. 2011. High-throughput illumina strand-specific RNA sequencing library preparation. *Cold Spring Harb Protoc* **2011**: 940-949.